TECHNISCHE UNIVERSITÄT WIEN
Vienna University of Technology

Diploma Thesis

Predicting failure of bone-anchored prostheses for transfemoral amputees using finite element models: A pilot study

---

carried out for the purpose of obtaining the degree of Master of Science (Dipl.-Ing.) submitted at the TU Wien Faculty of Mechanical and Industrial Engineering by

Ciara Burns, BSc
[redacted]

under the supervision of

Associate Prof. Dipl.-Ing. Dr.techn. **Dieter Pahr**
Institute of Lightweight Design and Structural Biomechanics, TU Wien

Co-Supervisor:

Univ.Ass. Dipl.-Ing. Dr.techn. **Alexander Synek**, MSc
Institute of Lightweight Design and Structural Biomechanics, TU Wien

Dipl.-Ing. Dr. **Emir Benca**
Department of Orthopedics and Trauma Surgery, Medical University of Vienna

Vienna, December 21, 2023 _____

Affidavit

I declare in lieu of oath, that I wrote this thesis and carried out the associated research myself, using only the literature cited in this volume. If text passages from sources are used literally, they are marked as such.
I confirm that this work is original and has not been submitted for examination elsewhere, nor is it currently under consideration for a thesis elsewhere.
I acknowledge that the submitted work will be checked electronically-technically using suitable and state-of-the-art means (plagiarism detection software). On the one hand, this ensures that the submitted work was prepared according to the high-quality standards within the applicable rules to ensure good scientific practice "Code of Conduct" at the TU Wien. On the other hand, a comparison with other student theses avoids violation of my personal copyright.

Vienna, December 21, 2023 _____

Abstract

Bone anchored prosthetics in transfemoral amputees offer an alternative to standard socket versions. However, the post implantation phase is extensive to ensure proper osseointegration and reduction of fracture risk. Computer simulations with finite element (FE) models could help to predict patient-specific implant failures and thereby reduce rehabilitation time and fracture risk. The goal of this study was to develop a workflow for a patient-specific FE model of a transfemoral amputee, with a threaded, endocortically anchored transfemoral prosthesis. The post-implantation, as well as osseointegrated state was modeled and compared. Further, a parameter study was conducted, evaluating the influence of FE-model simplifications.

Quantitative computed tomography (QCT) scans were performed on 24 human cadaveric femora. One specimen (Male, 71 years, left femur) with the thinnest mean corticalis in the shaft region, e.g., highest bone fracture risk, was selected for this study. The implant system used in this study was the Integrum OPRA system that utilizes a threaded bone-anchoring implant (all other systems are press-fit systems). A reference FE model was generated by extracting the bone geometry from the QCT scan, creating an amputation at a height of 350 mm and artificially inserting the implant system in the distal femoral shaft using computer aided design (CAD) software. The implant and the cortical bone in proximity to the implant were assigned non-linear material properties and the bone-implant interface was modeled including the threads of the implants. The post-implantation, as well as a fully osseointegrated state were simulated, by defining the bone-implant interface, either using frictional contact or a tie constraint. The parameter study included implant simplification, (1) thread removal and (2) use of a rigid implant. To analyze the potential for osseointegration, the models were loaded in a one-leg stance configuration with a physiological loading of 700 N and the micromotion between implant and the surrounding bone was evaluated. To estimate fracture risk, the load was increased until failure and the maximum force was recorded.

In summary, an FE modelling workflow was developed that allows patient-specific prediction of micro-motions and failure loads of osseointegrated implants in transfemoral amputations. For the investigated subject, the osseointegrated and the post-implantation model, hardly showed any differences in terms of their failure loads. In both cases, the bone-implant system failed at 4.6 kN. The failure was caused by yield of the replaceable abutment of the implant, which prevented any substantial damage to the bone. At the physiological loading of 700 N, the micromotion was well below limits required for good osseointegration. The parameter study showed that simplifications of the implant thread geometry do not affect the failure load, but the implant system must not be modelled as a rigid material. In a future study, the model could be validated using experimental data.

Zusammenfassung

Für transfemorale Amputationen gelten im Knochen verankerte Prothesen als eine gute Alternative zur standardmäßig durchgeführten Versorgung, durch sogennante Liner. Da eine gute Osseointegration für im Knochen verankerte Prothesen angestrebt wird und damit einhergehend das Bruchrisiko vermindert wird, ist die postimplantations Phase langwierig. Computersimulationen mit Hilfe von Finiten Elemente (FE) Modellen, könnten ein Implantatsversagen anhand von patientenspezifischen Modellen vorhersagen und damit die Rehabilitationszeit und das Risiko eines Implantatversagens reduzieren. Das Ziel dieser Studie war es einen Arbeitsablauf für ein patientenspezifisches FE-Modell einer transfemoral Amputation, welche mit einer gewindebehafteten endokortikal verankerndem Implantat versorgt wird, zu entwickeln. Die Phasen nach der Implantation und nach der Osseointegration wurden modelliert und evaluiert. Weiters wurde eine Parameterstudie durchgeführt, mit welcher die Einflüsse der FE-Modell simplifikation evaluiert wurden.

Quantitative Computertomographie (QCT) Scans, wurden an 24 anatomischen Präparaten humaner Femora durchgeführt. Das Präparat mit der dünnsten mittleren Kortikalis im Knochenschaft (Männlich, 71 Jahre, linkes Femur) und dem damit höchsten Bruchrisiko sowie das Integra OPRA System wurde für die anschließende Studie ausgewählt. Ein Referenz FE-Model wurde generiert, indem die Knochengeometrie aus dem QCT-Scan extrahiert, eine Amputation auf der Höhe von 350 mm generiert und das Implantatsystem virtuell mit Hilfe von CAD (Computer Aided Design) in den distalen Femurschaft eingesetzt wurde. Sowohl das Implantat als auch der kortikale Knochen in der Nähe des Implantats wurden mit nicht-linearem Material modelliert, zusätzlich wurde des Implantatsgewinde mitmodelliert. Die Phase der Postimplantation und Osseointegration wurde mit einem Reibkontakt zwischen Knochen und Implantat sowie einer idealen Verbindung simuliert. Die Parameterstudie wurde mit folgenden Vereinfachungen durchgeführt, (1) entfernen des Implantatsgewindes und (2) dem Verwenden eines rigiden Implantats. Um das Osseointegrations-Potential zu analysieren, wurde das Modell in der Einbeinkonfiguration und einer physiologischen Last von 700 N beaufschlagt und die Mikrobewegung zwischen dem Implantat und dem umgebenden Knochen evaluiert. Um das Bruchrisiko abzuschätzen, wurde die Belastung bis zum Versagen erhöht und die maximale Kraft wurde ermittelt.

Zusammenfassend wurde ein Arbeitsablauf für ein patientenspezifisches FE-Modell, welches die Microbewegung sowie die Versagenslast vorhersagt, entwickelt. Für den betrachteten Fall, zeigen die Modelle nach Implantation, bzw. nach erfolgter Osseintegration kaum einen Unterschied hinsichtlich der Versagenslast. In beiden Fällen versagt das Knochen-Implantat System bei 4.6kN. Das Versagen wurde durch die plastische Verformung eines austauschbaren Implantatteils verursacht, welches schwerwiegenden Knochenschaden verhindert. Bei der physiologischen Last von 700N, war die Microbewegung in den Modellen innerhalb der Limits die für eine gute Osseointegration erforderlich sind. Die Parameterstudie zeigte, dass das Weglassen des Gewindes die Versagenslast nicht beeinflusst, die vereinfachte Annahme eines rigiden Implantats hingegen die Ergebnisse stark beeinflusst. In einer weiterführenden Studie könnte das Modell durch experimentelle Daten validiert werden.

Acknowledgement

I would like to express my gratitude to everyone supporting me throughout my thesis. This thesis would not have been possible without the guidance of Dr. Emir Benca, Prof. Dieter Pahr and in particular Dr. Alexander Synek, who's relentlessness, flexibility and patience were extraordinary. His overview and exceptional knowledge was a constant source of information, contributing significantly to the thesis.

I would like to thank Dr. Lena Hirtler and Andreas Strassl, MSc, for supplying the specimens and conducting the CT-scans. Similarly, I want to express my gratitude to the Karl Landsteiner Privatuniversität für Gesundheitswissenschaften for equipping the calibration phantom.

Finally, I would like to thank my family and friends for their moral support and patience.

Contents

List of Figures

List of Tables

List of Abbreviations

3D	Three Dimensional
approx.	Approximately
BC	Boundary condition
BMD	Bone Mineral Density
CAD	Computer aided design
CT	Computed Tomography
Ct.Th	Cortical Thickness
DoF	Degree of freedom
e.g.	Example Given
FE	Finite Element
FEA	Finite Element Analysis
GV	Grey Value
HU	Houndsfield Unit
ILP	Integral Leg Prosthesis
kg	Kilograms
mm	Millimeter
OPL	Osseointegration Prosthetic Limb
OPRA	Osseointegrated Prostheses for the Rehabilitation of Amputees
QCT	Quantitative Computed Tomography
ROI	Region of Interest
RoM	Range of Motion
S1	Stage 1
S2	Stage 2
TF	Trans Femoral
vM-Stress	Von Mises-Stress
vs.	Versus

1 Introduction

1.1 Motivation

Limb loss continues to be prevalent [5], resulting in severe impacts on physical functionality and physiological wellbeing [6]. Equipping patients with a prosthetic limb may combat the impact on physical functionality [7, 8].
The conventional socket suspended prosthesis, involves various problems including skin irritations, poor suspension and excessive sweating [9]. Direct skeletal attachment, directly connecting the skeleton to the artificial limb, is considered as a solution to socket related problems [10].They ensure load transfer between the prosthesis and bone. For individuals with lower limb amputation, the load between the prosthetic leg and implant may be of substantial magnitude. Thus, an understanding of the bone-implant interface is essential.

The biomechanical behaviour of bone-anchored prostheses was subjected to several experimental, clinical and computational studies. The latter offering an inexpensive and fast alternative, allowing multiple parameter variations on the same patient-specific model, eliminating inter-specimen variability [11]. Currently computational models lack adequate experimental validation and do not make use of non-linear material models. Therefore, the findings can only be applied to clinical practice with certain limitations [11].

The goal of this thesis was to generate a workflow for a specimen specific finite element (FE) models, predicting the biomechanical behaviour of the bone-anchored prosthesis system OPRA. The post-implantation as well as osseointegrated state was modeled and compared. Further, a parameter study was conducted, assessing the influence of model simplifications. To facilitate future experimental validation of the FE simulation, the models mirror physiological conditions.

1.2 Transfemoral Amputations

Limb loss continues to be prevalent, despite medical advancements. 1.6 million people were estimated to be living with limb loss in 2005 [5]. Thus the epidemiology of limb loss is of vast importance and will be covered in the subsequent section.

1.2.1 Epidemiology

Limb loss can be divided into two subgroups, (1) major and (2) minor limb loss. Major limb loss is defined as e.g., transhumeral, transradial, transfemoral or transtibial amputations (Figure 1.1) [12]. Minor limb loss, is characterised as the amputation of the hand, toes or at mid-foot level [12]. Amputations most commonly relate to trauma, malignant tumors, vascular conditions, and birth abnormalities [13].

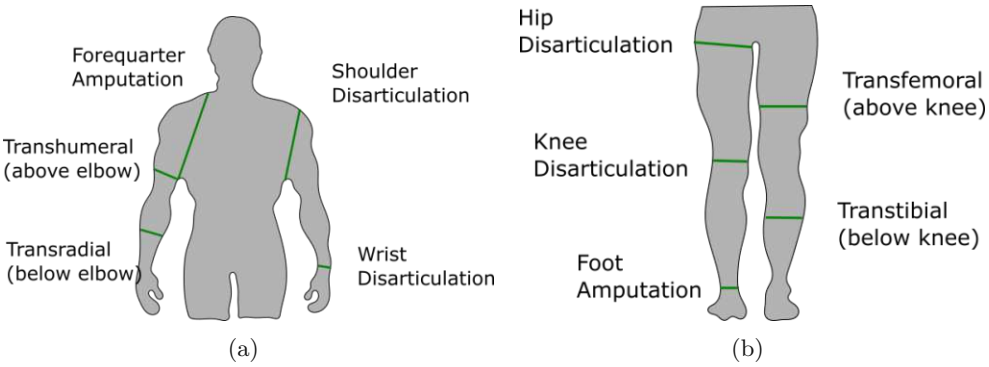

Figure 1.1: Levels of major limb amputations in (a) upper extremities and (b) lower extremities [14]

Transfemoral amputations are among the most common amputation levels for the lower limb [14]. Multiple factors, such as cognitive ability, mobility goals, endurance and level of amputation must be considered when determining the eligibility of a patient for a prosthetic. Lower extremity prosthetics are more likely to be accepted, when fitting patients within the first three months before patients learn to accomplish tasks without a prosthetic [14]. A basic overview of the femur anatomy as well as treatment methods after amputation are given in the subsequent sections.

1.2.2 Femur Anatomy

The upper leg is constituted by the femur, the knee joint on the distal end and the hip joint on the proximal end (Figure 1.2).

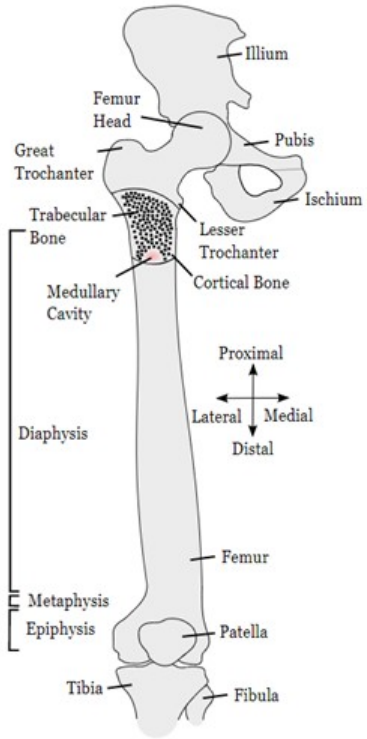

Figure 1.2: Femur Anatomy of bones including the knee and hip joint [1]

The femur is characterized by a prominent distal anatomical landmark, the great trochanter, a large irregular eminence, located lateral and slightly posterior. The lesser trochanter, an additional landmark, is a conical eminence located medial and posterior on the femur [1].

Long bones such as the femur, consist of an epiphysis, metaphysis and diaphysis. A dense cortical bone shell filled with spongy, trabecular bone, most pronounced in the epi- and metaphysis. The diaphysis is predominantly constituted by cortical bone as well as the medullary cavity, where red and yellow bone marrow is stored [15].

On the distal end the femur, patella and tibia form the knee joint [16]. At the proximal end, the femur and the acetabulum constitute the hip joint. Three bones come together to form the acetabulum, the os illium (40% of acetabulum), os ischium (40%) and the os pubis (20%) [17].

The thigh muscles are devided into (a) anterior, (b) medial, (c) posterior and (d) gluteal components. With the femur situated in the anterior section.
The muscles included in the anterior compartment are the M. pectineus, M. iliopsoas, and the M. sartorius used for hip flexion and knee extension. The muscles in the medial compartment include the M. adductor longus, M. adductor brevis, M. adductor magnus, M. gracilis and M. obturator externus muscles. They are mainly used for the hip adduction. The M. biceps femoris, M. semitendinosus, and M. semimembranosus constitute the posterior section, mainly needed for hip extension and knee flexion [18].

1.2.3 Amputation Procedure

The following chapter briefly summarizes the amputation procedure as described by Gottschalk et al. [17]. The reader is referred to the original publication ([17]) for more details. The gait of an transfemoral amputee, is known to be 65% more energy consuming. This severity can be reduced by performing the amputation with biomechanical principles and muscle preservation in mind. The residual length should be maximised, as functional ability and better prosthetic adhesion can be ensured.
The biomechanics of the healthy two legged stance has been defined by an axis running from the center of the femoral head through the center of the knee. Normal anatomical alignment is therefore adduction, which allows the gluteus medius and minimus as well as the gluteus medius and tensor fasciae latae to reduce the lateral motion of the center of mass. Most transfemoral amputees do not have the natural anatomical alignment with the tibia, resulting in mechanical and anatomical misalignment. The shaft axis is in abduction, increasing the energy consumption. As only the adductor magnus has an insertion in the mediodistal third of the femur, therefore loosing this attachment results in an abduction.

In general before amputations begin the skin flaps should be marked to ensure a posterior suture line. After making the incision, the major vessels and nerves must be isolated. The vesseles should be cut at the same level as the bone, whereas the nerves should be two to four cm proximal to that. The central vessel is then secured around the nerve. In a next step the muscles must be identified and then cut according to the specified location. The femur is exposed and cut with an oscillating blade, cooled with saline. Two or three drill holes are made on the lateral cortex, one cm from the distal end of the femur. The adductor magnus tendon is then sutured to the residual femur via the drill holes, while

holding it in maximum adduction. Next the quadriceps is sutured to the femur via the posterior drill holes, with a fully extended hip to prevent hip flexion contracture. The remaining fascia is then sutured as dictated by the skin flaps.
An elastic bandage is wrapped around the residual limb to reduce swelling and discomfort. The patient should be immobilized in a wheelchair while the wound is healing after approximatly two weeks the sutures may be removed.

1.2.4 Treatments

Transfemoral amputation has been described to have a severe impact on physical functionality, physiological wellbeing and social interactions [6]. After transfemoral amputation, pain as well as reduced mobility, loss of freedom, quality of life reduction, social discomfort, body image changes and subsequently higher frequency of depression are experienced [19, 20, 21]. Studies show that equipping patients with a prosthesis may combat the previously mentioned experiences and help regain physical mobility[7, 8]. Determining if a patient is an appropriate candidate for a prosthesis, is dependent on multiple factors, including mobility goals, cognitive ability and level of amputation [14].

The bodies compatibility with a prosthesis is limited by the patients residual limb and prosthesis interface [22]. The two most common interfaces are the socket and direct skeletal attachment. Both options will be discussed in the remainder of this chapter.

The conventional socket-suspended prosthesis, is the proven standard for treating lower extremity amputation. Socket design is dependent on the patients specific requirements and anatomy [23]. However two variants are most commonly used,the quadrilateral socket as well as the current standard ischium containing socket [24] (Figure 1.3).

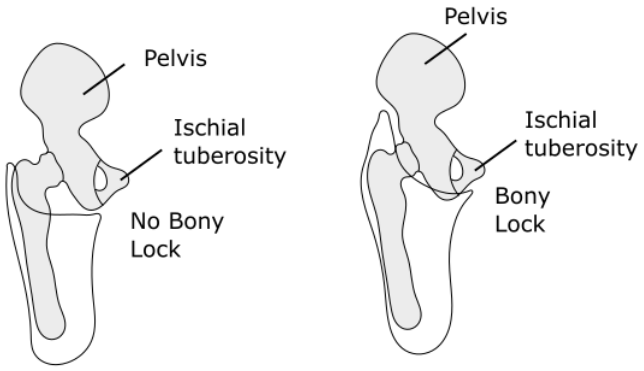

(a) (b)

Figure 1.3: Most commonly used socket suspended prosthesis types: (a) quadrilateral and (b) the current standard ischium containing socket [24]

Quadrilateral sockets were introduced in the 1950s, by the department of mechanical engineering at the university of Berkley (California, United states of America). The four-sided shape of the socket applies pressure and counter pressure to facilitate comfortable load bearing, via the soft tissue and underlying structures [24].

In 1975, Long et al. [25] reported that the femur adduction did not match the quadrilateral socket. Thus the medial-lateral dimension of the socket was narrowed to gain better control of the femur. Further, the ischium was included in the socket, as research suggested, that the socket tends to move laterally on bearing weight [25]. The ischium containing socket is currently the standard for transfemoral amputees.

The socket suspended prosthesis involves various problems, including skin irritations (chafing, sores and ulcers), poor suspension, due to short residual limbs and excessive sweating [9]. A survey conducted with 90 transfemoral amputees, highlighted, that 72% were experiencing heat/sweat problems in the socket and 62% had sores and skin irritations [26]. Direct skeletal attachment, a method allowing the direct connection of an artificial limb to the skeleton, is considered as a solution to problems related to socket suspension [10].

Bone anchored system are based on osseointegration of the fixture, enabling physiological load bearing, essential for the implant system. A direct structural and functional connection between the host bone and non-biological implant is vital [27].

Osseointegration begins with the formation of a hematoma, allowing clot formation at the surface of the implant. A fibrin matrix, serving as a scaffold for osteogenic cells is stimulated within this clot. The calcified matrix further transitions to lamellar bone, which responds to mechanical loading and undergoes morphologic remodeling, similar to the native host bone [28].
The promotion of osseointegration is subject to a variety of factors, one of which is implant design. The biological compatibility of the implant material as well as the surface roughness are essential for the adhesion of monocytes, which form the fibrin matrix. Early implant stability is crucial in preventing excessive micro- and macro-motion at the bone-implant interface, subsequently leading to aseptic loosening and eventual failure [28].

Benefits compared to socket prosthesis include the enhancement of proprioception and osseoperception, allowing an increased awareness of the limb positioning in space as well as heightened sense of feel [29]. The prosthesis wear time and daily steps are increased due to more comfort and wider range of motion [30].
Implant failure is most commonly caused by infection, fracture or mechanical complications, in the worst case resulting in implant removal. Infections remain the biggest risk, most are superficial occurring at the implant-skin interface and can be treated with a short course of oral antibiotics. Deeper infections however often need to be treated surgically. Additionally the relative motion between the implant and skin can result in the formation of granulation tissue. These problems are managed conservatively by daily wound cleaning [31].

Implant material, design and surface coating determine the success of osseointegrated systems. The three clinical systems currently available are [32]:

(i) Threaded endocortical implants OPRA (Osseoanchored Prostheses for the Rehabilitation of Amputee, Integrum AB, Molndal, Sweden)

(ii) Porous-coated press-fit implants OPL (Osseointegrated Prosthetic Limb, Permedica, Merate, Italy)

(ii) Porous-coated press-fit implants ESKA (Endo-Exo Femur-Prosthesis, ESKA Orthopaedic, Lübeck, Germany; also known as Integral Leg Prosthesis (ILP))

The main differences between the press-fit and threaded implants are (1) the fixation method where the OPRA system makes use of a threaded bone anchorage element, both the OPL and ILP use a porous surface without threads, (2) the intermedullary length of 80mm for the OPRA implant, 140-180mm for ILP and the OPL has 160mm (3) the rehabilitation protocol of the OPRA is slower compared to the OLP and ILP, indicating the mechanical stability between bone and implant may form later.[32]

This study includes the OPRA implant system (Osseoanchored Prostheses for the Rehabilitation of Amputee), thus it will be explained in more detail in the following section.

1.3 OPRA Implant System

The first transfemoral surgery of the Osseoanchored Prostheses for the Rehabilitation of Amputees (OPRA) Implant system was performed by Dr. Per-Ingvar Brånemark and Dr. Björn Rydevik in 1990, representing a milestone in implant treatment [32].
R. Brånemark standardized the implant system, surgical technique, and postoperative rehabilitation protocol in 1998. It was named OPRA [33]. The following sections give an overview of the OPRA design, surgical procedure and rehabilitation.

1.3.1 Implant Design

The implant system consists of 3 parts, the fixture, abutment and abutment screw. The fixture is an anchoring element, externally threaded for engagement with the patient's bone cortex. The titanium alloy fixture, undergoes a surface treatment trademarked BioHelix^{TM} introducing a nanoporous structure for improved osseointegration [34]. The titanium alloy abutment is attached distally by press-fitting and penetrates the skin (Figure 1.4). It is secured by the third element, the abutment screw made of titanium alloy [33].

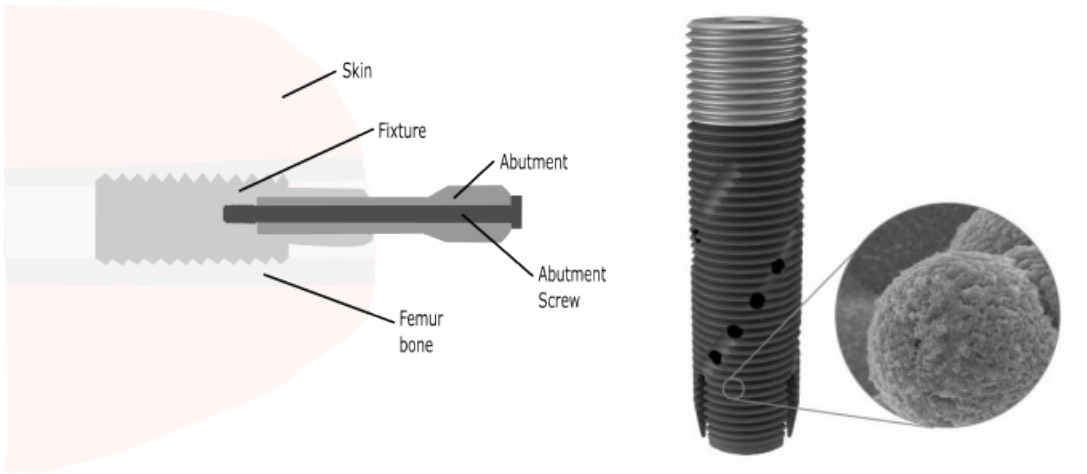

(a) (b)

Figure 1.4: OPRA implant (a) basic implant design with three main components the abutment, abutment screw and the fixture [2] (b) design of the fixtures trademarked thread named BioHelix^{TM}[3]

External loads are transferred from the prosthesis to the abutment, then the fixture and

bone. When exposed to excessive loads, the system was designed to ensure the abutment and abutment screw breakage before the fixture, avoiding major surgical intervention. Additionally, a safety device is placed between the distal end of the abutment and prosthesis, releasing during exposure to fracture inducing loads. [32]

1.3.2 Surgical Procedure

According to the OPRA protocol, a two-staged surgery is performed. In Stage 1 (S1) the femur stump is prepared for fixture insertion. The medullary canal is drilled to a specific diameter, accommodating the chosen implant size, followed by thread tapping. The fixture is inserted into the canal, ensuring close contact of the fixtures threads to the cortex. Inhibiting micro- motion and achieving good post surgery stability is essential for osseointegration [28, 33]. Placing the fixture into the bone 20mm countersunk addresses the problem of distal bone resorption, which can be observed when placing the fixture flush with the distal bone [32].

To ensure osseointegration, even for non-optimal post surgery stability, a 6-month healing period is required prior to Stage 2 (S2) surgery. The stump remains unloaded during the period, but the usage of a socket prosthesis is permitted.

In Stage 2 (S2) the abutment is placed on the distally located press fit system of the fixture, by applying pressure via the abutment screw. To reduce future soft tissue problems thin, hair follicular free and immobile skin around the abutment is essential. Therefore, the muscle endings are sutured to the periosteum five to ten millimeters proximal to the bone end, additionally subcutaneous fat is removed [33, 28].

1.3.3 Rehabilitation Protocol

Mobilization is carried out using the standardized rehabilitation program [4] stated in the following chapter and visualised in the timeline (Figure 1.5).

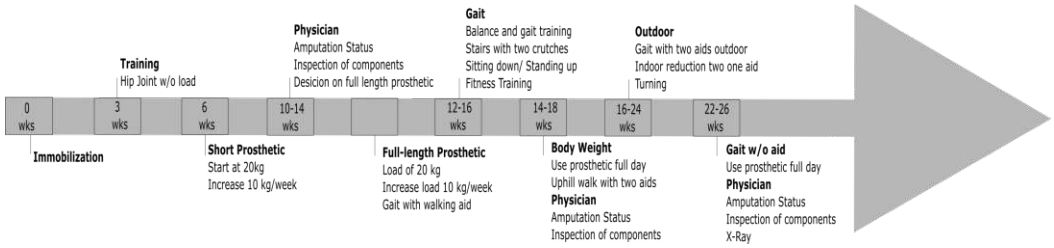

Figure 1.5: Timeline of the OPRA rehabilitation procedure [4]

Two weeks post S2, the transfemoral amputee begins active movement of the hip joint without load. At 4-6 weeks initial loading with a short training prosthesis, that only reaches the knee joint begins. An initial load of 20kg is applied for 2x15 minutes per day, discouraging rotational movement. The load is increased by ten kilogramms per week until the full bodyweight is reached, if pain occurs the load may be reduced. Assuming full bodyweight can be applied and training is conducted without pain a general exercise program may be performed in week 10-14, increasing the hip RoM (range of motion) and muscle strength. Following the physicians decision, a full-length prosthesis can be used. An initial load of maximum 20kg may be applied for maximum 2x60 minutes indoor, while using walking aids (parallel bars or 2 crutches). The weight should be increased by ten kg

per week. At week 12-16 the amputee may begin balance, gait, sitting down/standing up and stair training, two crutches must still be used. At week 14-18 the prosthesis can be used for the whole day, additionally the full bodyweight may be transferred while standing and the patient may walk uphill, while using support. From week 16-24 the support can be reduced to one while walking inside, on rough terrain two crutches must still be used. At week 22-26, if the gait can be performed in training without the usage of crutches, the treating physician judges the patients bone quality, deciding if the mobilization program must be continued.

1.4 State of the Art

Numerous different studies on bone anchored implant systems have been conducted. Currently, there is no consensus as to whether studies on synthetic or cadaveric bone, or finite element studies provided results, best represent the clinical experience [11]. The following section offers the basic knowledge about the study types as well as an overview of the current research state.

1.4.1 Clinical Studies

Clinical studies aim to determine the safety and efficiency of medical treatments. The in vivo measurements are limited to the force applied on the abutment in different loading scenarios such as walking and falling. Additionally follow up studies were conducted, evaluating the implant failure rate, quality of life, infections and mechanical complications.

Studies measuring the load applied on trans-femoral bone anchored prosthesis have been conducted with the use of load transducers between the fixation and prosthetic knee. The loading scenarios included gait [35, 36, 37], ascending and descending of stairs and a ramp [37], walking in a circle [37], falling [38] and the rehabilitation protocol [39].

The most commonly used tool to evaluate prosthetic mobilization in literature is the Questionnaire for Persons with a Transfemoral Amputation (Q-TFA)[40]. Studies were performed with patients implanted with OPRA systems and press-fit implants (implant types: OPL, ILP), all resulting in similar or improved levels when considering quality of life over time [41, 42, 43, 44, 45]. Comparison of 22 patients with osseointegrated ILP prosthetics to 19 age-matched socket prosthesis users, showed a significantly higher quality of life (mean global Q-TFA score) in the osseointegrated patients [46].
Numerous studies on infections have been conducted, reporting that most infections are superficial, thus no surgery was needed [41, 47, 48]. However, studies including longer follow up schedules reported that risk of deep infections increased over time [42, 49, 50].
The severity of mechanical complications increases significantly with the prolonged prosthesis usage. Brånemark et al. [41, 42] reported 8% of the abutment and abutment screws failed within 2 years, increasing to 29% after 5 years. A positive relationship between a higher activity level and the number of mechanical complications can be shown [45].

1.4.2 Experimental Studies

Experimental studies are typically conducted on synthetic or cadaveric human or animal bones and always simplify the physiological situation. The ability to observe different variables compared to clinical studies offers a major advantage [11].

Very few experimental studies on bone anchored implant systems have been conducted. Tomaszewski et al. [51] conducted an experimental assessment of a bone anchored implant system, with an improved implant design. Seven specimens were implanted and loaded with forces measured in-vivo on a patient with an OPRA implant. The data collected by twelve strain gauges and an additional finite element model, aimed at the determination if the implant design has the capability to reduce strain shielding.

Welke et al. [52] conducted bending stiffness and axial pull-out experiments on eight human and sixteen synthetic bones. Significant differences between human and synthetic specimens were reported in respect to the maximum bending moment.

1.4.3 Computational Studies

Computational studies simulate biomechanical experiments computationally, by solving mathematical models numerically. Mechanical and biomechanical behaviours of solids can be predicted using finite element (FE) analysis, making it a standard tool in engineering and in the biomechanical field [53, 11].

In general the FE method solves problems numerically, for which analytical solutions are unobtainable [53, 54, 55]. The method divides the geometry into a finite number of building blocks (elements) that are defined and interconnected at points (nodes), resulting in a mesh [56]. Material properties are defined for each element of the mesh. Together with boundary conditions (e.g., nodal loads and displacements), a global system of equations can be established and solved for unknown displacements and loads. Therefore, the stress distribution within the element and subsequently throughout the entire volume can be obtained [55].
A prerequisite for the FE method is an accurate bone representation, including the geometry and material behavior. As bone is a highly hierarchical and heterogeneous structure, mapping the bone-model's material presents a major challenge [57]. For that purpose, commonly a computed tomogrphy (CT) scan is conducted and material properties are assigned to each element depending on the local bone structure (e.g., local density) [58].

Numerous FE analysis have been conducted, modeling osseointegrated implants, with linear materials, evaluating the von Mises stress while exerting gait loads, observed in clinical studies [59, 60].
Prochor et al. [61] compared a threaded OPRA implant to a unthreaded press fit implant by applying an axial force. The bone was modeled as a cylinder with orthotropic materials, whereas the implant was modeled as isotropic. The fully osseointegrated as well as post implantation state were modeled, with a tied constrained and a friction contact of 0.4 between the bone and implant. The von Mises stress as well as axial implant displacement were evaluated at different load steps, no failure load was evaluated.
In another model, Tomaszewski et al.[62] assessed the OPRA implant on bone failure post operation and after osseointegration. The bone elements were modeled according to their ash density, a force observed during a gait cycle was applied distally on the implant, whereas the proximal part of the femur was fixed. The friction coefficient used for the post implantation state was 0.4, whereas the osseointegration was modeled with a tied constraint.
Thesleff et al. [63] created an FE model, with different cortical thicknesses and thread heights. The bone was fully bonded with the implant and modeled with a transversely isotropic material. The implant was fixed into a cylindrical bone shaft and fixed proxi-

mally, while the load was applied distally on the implant. Cortical thickness was shown to be the most influential factor on the stress and strain of the model. 36% to 44% bone stress reductions were observed with a cortical thickness increase from two to five mm. The thread depth had larger effects on the maximum stress than the thread radius.
However, none of the FE simulations, known by the author included non-linear material models and adequate validation.

1.5 Gaps and Thesis Goals

Bone anchored systems, such as the OPRA system, have benefits compared to the conventional socket systems. The proprioception and osseoperception, increasing the awareness of limb positioning, as well as the increased wear time are beneficial, even though drawbacks such as infections, fracture and mechanical failures may not be disregarded.
Finite element studies are a good tool to provide deeper insight into the biomechanical behaviour. Multiple variables can be virtually tested on the same patient-specific model, eliminating inter-specimen variability. Drawbacks of biomechanical experiments can therefore be eliminated. The systems weakest links can be revealed by the finite element analysis, providing an insight into the implant system.
However, major limitations of previously published FE models, can not be disregarded.

1. The models were not validated: Not validated FEAs are useful for comparison of parameters and an understanding of the bone-implant interface. Their clinical relevance on the other hand is impaired.

2. Simplified models: Finite element models, always offer a simplified virtual model of the reality. Simplifications include:
   - Material: Mostly linear materials were used that do not capture local bone damage or plasticity [59, 60].
   - Geometry: Implant simplifications often include the removal of thread [62]
   - Failure prediction: Bone and implant failures as well as micromotion are often not predicted in FE models [62, 32].
   - Interfaces: Post - implantation states are modeled with a frictional constraint, osseointegration with a tied constraint, both simplifying the actual bone/implant contact [61, 62].

The influence of the simplification parameters used in literature have not been studied and compared to a reference model at physiological or failure load. In this pilot study, some of the above gaps shall be filled. The primary goals of this thesis, were defined as follows:

(i) *Creation of workflow from CT-data to a FE-model:* Enabling patient-specific models, that predict micromotion and bone/implant failure.

(ii) *Comparison of biomechanical behavior directly after implantation vs. after osseointegration:* The biomechanical behaviour is predicted both at physiological load and failure.

(iii) *Parameter Variation:* Test how simple the model can be to capture the reference models biomechanical behaviour at physiological loading and failure

Specifically, the simplifications include:

(a) Modelling the inferface without threads of the fixture

(b) Modelling the implant as rigid rather than elasto-plastic

2 Material and Methods

This study was based on a specimen specific FE model with an artificially created amputation as well as virtually inserted OPRA implant system (Integrum AB, Mölndal, Sweden). The outline of the study design is shown in Figure 2.1.

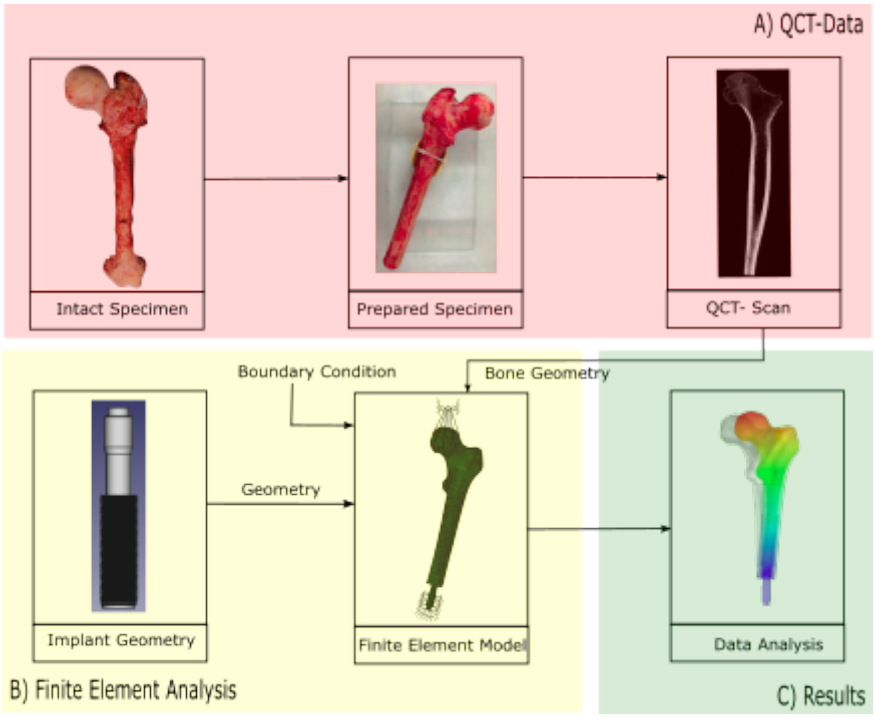

Figure 2.1: Outline of the study design

Twenty-four fresh frozen anatomic human femoral specimens (mean age: 73 years; standard deviation 4 years; 16 male and 8 female; 12 left and 12 right femurs) were cut and scanned using a quantitative computed tomography (QCT) scanner. The QCT scan of one selected specimen as well as the implant geometry were utilized to create an FE model representing the femoral bone with the implanted OPRA system. The biomechanical behaviour post-implantation (primary stability) as well as after osseointegration (secondary stability) was analyzed at a physiological load to assess micromotion and then loaded until failure. Additionally, the simplified models feasibility was evaluated with a parameter variation study by comparing the predictions to a reference model. This pilot study is part of a larger study including experimental measurements and was approved by the Ethics Committee of the Medical University of Vienna (1876/2019).

The following sections are structured according to Figure 2.1, the image acquisition and processing (A), finite element analysis (B) and data analysis (C) is presented in more detail.

2.1 Image Acquisition and Processing

The content of the following section outlines the image acquisition using a QCT-scanner, as well as the image processing. All necessary steps are displayed in Figure 2.2.

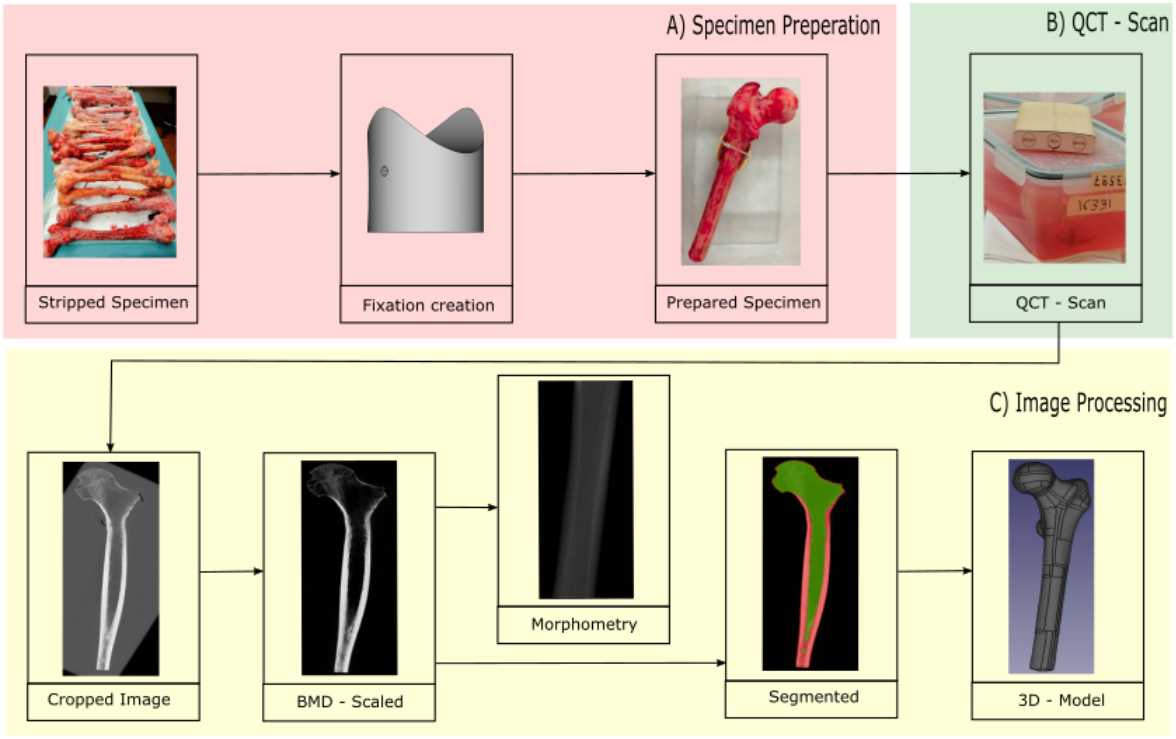

Figure 2.2: Outline of the image acquisition and processing

First, the specimens were prepared (A), QCT-scanned (B) and afterwards the images were processed to create separate 3D models of the cortical and trabecular bone (C).

2.1.1 Specimen Preparation

Twenty-four frozen femora were obtained from the Center of Anatomy and Cell Biology (Medical University of Vienna, Austria) and stored in a freezer at -18°C. The study was approved by the Ethics Committee of the Medical University of Vienna (1876/2019). All specimens were stripped of their soft tissue, cut to a uniform length of 400mm and placed back in the freezer.

The bones were horizontally aligned by custom bone fixations. The materials were chosen to absorb a small amount of X-rays and show little contrast in the scan. The stumps were cast with a polyurethane mixture (SG141/PUR145, FDW Handelsgesellschaft, Liezen, Austria) in a cylindrical mold, with a round indentation on the top. After curing, the round indentation on the top was carved to fit the individual specimens, additionally a hole was drilled for the cable tie (Figure 2.3). The fixation stumps were glued to plastic boxes and the specimens were fixed with cable ties, distal of the lesser trochanter. The bone was submerged in saline solution, to avoid artefacts caused by air bubbles and to simulate a clinical scenario.

(a) Specimens (b) Prepared Specimen (c) Prepared Specimen

Figure 2.3: (a) Specimens obtained from the Center of Anatomy and Cell Biology, (b) and (c) specimens stripped of their soft tissue and aligned with custom made bone fixations for the QCT scan

2.1.2 QCT Scanning

QCT scanning of the prepared specimen was conducted with a Brilliant CT 64-Channel Scanner (Phillips, Amsterdam, The Netherlands) and a slice thickness of 0.6mm, a tube voltage of 100kV and tube current 253mA. A three chamber calibration phantom (BDC Phantom, QRM GmbH, Moehrendorf, Germany) placed on top of the first of four specimens included in every scan, ensured density calibration and will be explained in further detail in the following section (Figure 2.4).

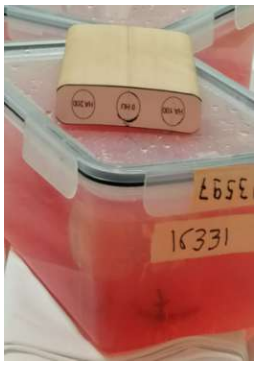

Figure 2.4: Samples submerged in saline solution for the QCT scan, including the phantom on top of the box

2.1.3 QCT Image Processing

The QCT scan was processed to obtain different 3D images for each specimen: A bone mineral density (BMD) scaled image, a segmented image separating the cortical and trabecular bone regions. A triangulated surface mesh of each region was generated and subsequently converted into a smooth, spline-based boundary representation that can be further processed in computer aided design (CAD) software. All steps if not mentioned otherwise were performed in Medtool (Dr. Pahr Ingenieure e.U., Pfaffstaetten, Austria; Version 4.5) a script management tool developed at the TU Wien, Austria.

First the original QCT images were re-sampled to an isotropic voxel size of 0.4 mm. Further they were cropped to the region of interest (ROI) containing only the bone, by manually choosing the bounding box coordinates.

The obtained CT-images are given in Houndsfield Units (HU), a relative quantitative measurement of density. Specifically, the radiation absorption coefficient is used to produce a greyscale image, which is proportional to the physical density. Typically distilled water has a value of 0HU, where as air is defined at -1000HU. Denser tissues with greater X-ray absorption, have a positive value and appear bright in the greyscale [64]. To create a QCT-image with Bone Mineral Density (BMD) in hydroxyapatit mass per cubic centimeter (mgHA/cm^3) the calibration phantom is used. It includes three rods with known HU and BMD, allowing a linear calibration relationship to be formulated.

The phantom includes 3 calibration chambers in the shape of circular rods, with known BMD of 0, 100 and 200 mgHA/cm^3. The chambers are selected manually with ROIs and labeled, to further correlate the known BMD. Additionally the density was limited to a range of 0-1400 mgHA/cm^3, to exclude noise and artefacts. The linear calibration relationship including the applied limits is shown in Figure 2.5(a), the red dots denote the known BMD of the calibrations phantom chambers. Figure 2.5(b) shows the grey value distribution in the phantom area previously cropped.

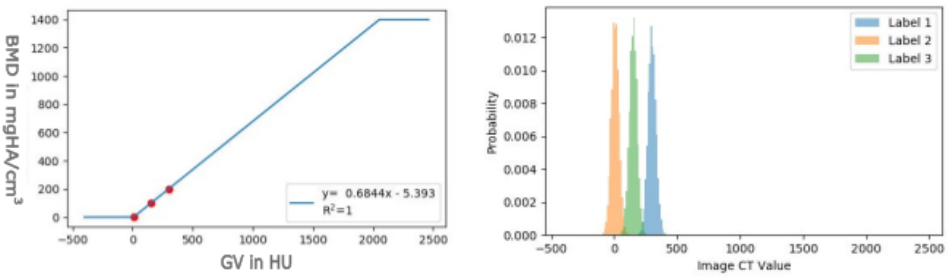

(a) Regression (b) Histogram

Figure 2.5: Calibration parameter output in Medtool (a) regression showing the calibration relation between the BMD and GV, where the red dots denote the known values of the phantom (b) the grey value distribution in the phantom area

The obtained image was further segmented into separate cortical and trabecular bone regions, with a custom algorithm based on region growing and morphological filter. Further details are described in [65], the segmentation threshold chosen for this specimen is 130. A cleaning step was required pre-segmentation, removing bone fragments contained in the remaining soft tissue surrounding the specimens. The cortical and trabecular bone regions were then segmented separately with the above mentioned algorithm. In the last step the images were combined creating the segmented 3D bone image, containing trabecular and cortical bone with different HU (Figure 2.6).

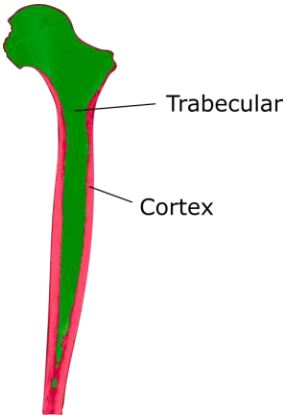

Figure 2.6: Femur segmented into separate cortical and trabecular bone regions, with a custom algorithm

In the following steps the outer surface was meshed and further converted into a volume. All the following steps were done separately on the full (cortical and trabecular region) as well as the trabecular bone. Firstly, a Medtool plug-in from the University of Cambridge (Machine intelligence Laboritry, Department of Engineering, Cambridge, United Kingdom) was used to create a triangulated iso-surface. This was further exported to Recap Photo (Autodesk Inc., San Rafael, California, United States of America), creating a surface mesh with approximately 300 quadrilateral faces. To further process the surface in CAD software, it was converted into a smooth spline-based surface and exported in suitable format, e.g., as a .step file. This was done in Fusion 360 (Autodesk Inc., San Rafael, California, United States of America) by converting the surface mesh to a volume with boundary representation using B-splines and then exporting it (Figure 2.7).

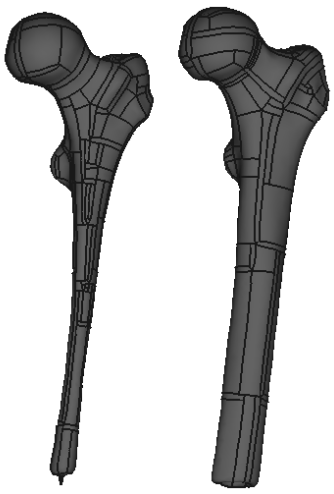

Figure 2.7: Spline-based boundary representation of the bone geometry - trabecular region and full bone (cortical and trabecular region)

Additionally to extract the bone geometry, the morphometry of the specimens was evaluated, in particular the average cortical thickness and average BMD, to select a suitable specimen for this study. Therefore the specimens were divided distally of the lesser trochanter. The proximal part was used for the BMD calculation, where as the distal part was used for the evaluation of the cortical thickness. To reduce the error, due to image processing, in the most distal part of the bone, it was cropped, leaving only the shaft.

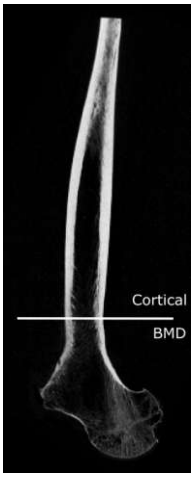

Figure 2.8: Proximal and distal region of one exemplary femur to evaluate proximal bone BMD and distal shaft cortical thickness.

The average BMD of the proximal femur was calculated, with following equation:

$$BMD_{\text{average}} = \frac{1}{n} \sum_{i}^{n} BMD_i \tag{1}$$

Where BMD_i is the BMD value of each voxel inside the bone volume and n is the total number of voxels within the bone volume.

The cortical thickness was evaluated with a custom Medtool function where the maximum, mean and standard deviation values are returned.

The bone with the lowest mean cortical thickness (Bone ID 13373) was chosen for further analysis/ FE-model creation (Male, 71 years, left femur). Table 2.1 gives an overview of the mean bone mineral density (BMD) and minimum, maximum and mean cortical thickness (Ct.Th) values.

Specimen ID	Mean BMD in mgHA/cm^3	Min Ct.Th in mm	Max Ct.Th in mm	Mean Ct.Th in mm
11057	327.43	0.80	10.55	7.99
11058	341.55	2.88	11.31	8.51
12959	291.40	0.80	10.18	8.08
12960	273.84	4.00	10.15	7.84
13279	248.93	3.30	11.31	8.45
13280	229.87	0.80	10.67	7.87
13373	**262.99**	**0.80**	**9.33**	**6.34**
13374	251.09	1.60	8.50	6.54
13546	299.23	3.39	10.91	8.52
13547	284.94	3.29	10.88	8.22
13567	344.51	1.13	10.46	7.96
13598	360.25	1.13	10.99	7.96
13834	304.99	0.80	10.43	8.51
13835	321.51	3.48	10.73	8.81
15709	287.44	2.26	9.09	6.68
16331	364.14	3.39	11.89	8.77
16332	359.28	3.39	12.29	8.68
16333	289.62	1.60	9.26	6.60
16334	286.73	1.13	9.63	7.04
16338	315.77	0.80	10.67	8.03
16339	282.32	1.13	9.93	7.87
16608	267.83	0.80	10.40	7.62
16609	297.44	0.80	10.52	7.29

Table 2.1: Morphometry - Mean bone mineral density (BMD) and minimum, maximum and mean cortical thickness (Ct.Th)

2.2 Finite Element Analysis of Reference Model

The goal of the finite element analysis was to analyse the biomechanical behavior of the bone-implant system in the post-surgery and osseointegrated state using a detailed model. In addition, the influence of model simplifications with respect to the reference model were evaluated. In the following chapters the most complex model, later referred to as reference model, will be discussed. The simplifications will be explained in more detail in chapter 2.3.2.
The following section is outlined in the graphical abstract (Figure 2.9) and will be discussed in more detail in the following sections.

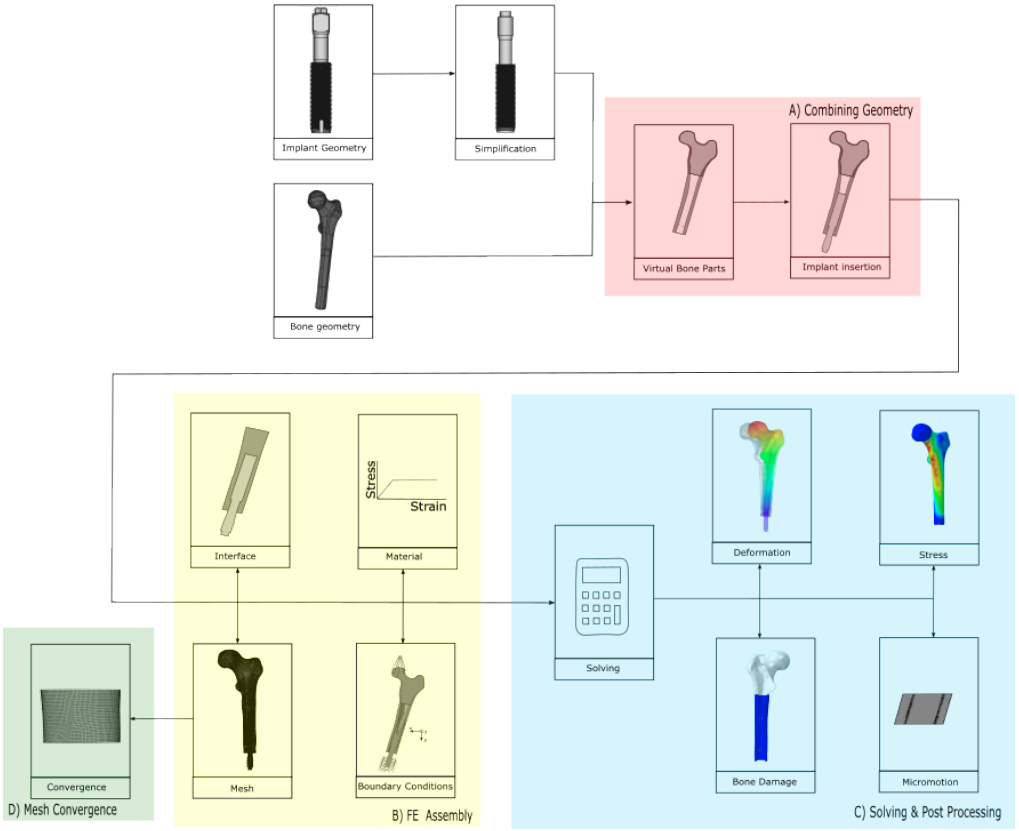

Figure 2.9: Outline of the FE model creation, solving and post-processing

First the bone geometry was combined with the modified implant geometry (A), then the mesh, material, interfaces and boundary conditions and load were applied (B), before solving and postprocessing (C). Additionally the mesh convergence was evaluated (D).

2.2.1 Combining Bone and Implant Geometry

A combined model containing the trabecular and cortical bone as well as the implant is essential for the FE analysis. For this purpose the modified implant geometry was virtually implanted in the bone according to the standardised OPRA surgical procedure [33]. All steps if not mentioned otherwise were performed in FreeCAD (Version 0.20).
The implant geometry was obtained from Integrum AB (Molndal, Sweden) and further simplified, to ease the meshing procedure and save computational time. The following modifications were performed (marked in red in Figure 2.10):

- Fixture was threaded axial
- Fixture simplification by removing holes
- Abutment simplified by changing the shape to cylindrical
- The different parts of the implant, detailed in chapter 1.3.1 Implant Design, are modeled as one part, allowing no movement between each other.

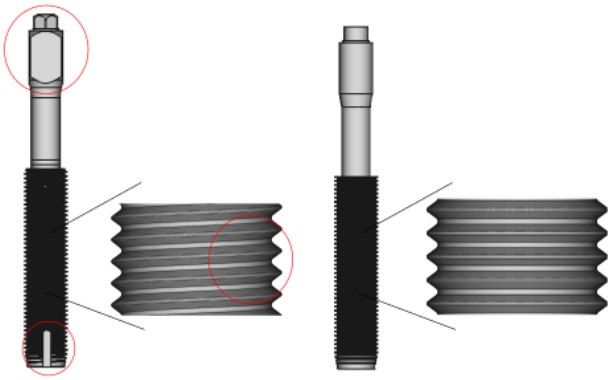

Figure 2.10: Simplifications of the original implant geometry, including (1) an axial thread (2) abutment geometry changed to cylindrical (3) removal of proximal hole (4) modeling as one part

Figure 2.9(A) gives an overview of the steps performed while combining the geometries. Different bone parts (Figure 2.11) were subdivided in CAD, as varying materials were applied to each part during the FEA. First a boolean cut of the trabecular bone and full bone model, obtained after image processing, was performed, generating the bone cortex. The bone was shortened to a total length of 350mm, by removing the distal end. The bone was divided into a proximal and distal part, by cutting it just distal of the lower trochanter. The proximal trabecular bone was constituted by filling the proximal cortex.

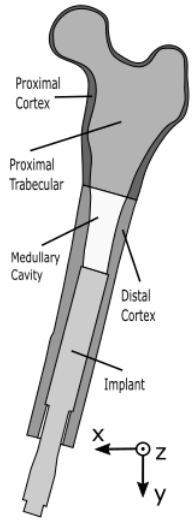

Figure 2.11: Overview of virtually created bone parts, including (1) the proximal cortex, (2) proximal trabecular, (3) the distal cortex and (4) the implant

Implantation was based on the standardised OPRA surgical procedure. First, a cylindrical element (ø16.5mm; length: 100mm) was manually aligned posterior/anterior as well as lateral/medial in the medullary cavity to ensure good implant positioning. The 80mm long implant can therefore be countersunk into the hole, as previously mentioned. A boolean cut was performed with first the element and then the implant creating the threads on the hole.

2.2.2 FE Model Assembly

In order to generate a FE model it is necessary to create a mesh, assign a material, define the interfaces and impose boundary conditions, which are outlined in the remainder of this section. The models are created with Abaqus Version6, 2020.

A first-order tetrahedral mesh (C3D4) was generated on the individual bone parts. A seed size of 1.1 was chosen according to the mesh convergence study covered in more detail in chapter 2.2.4. The number of elements for each individual part can be seen in Table 2.2.

Proximal Cortex	**Proximal Trabecular**	**Distal Cortex**	**Implant**
176,502	417,385	279,113	119,189

Table 2.2: Number of elements of the virtually created individual parts

Each of the individual bone parts were assigned with a different material model, outlined in Table 2.3. The distal cortex was modeled as an elastic-viscoplastic damageable material based on the model proposed by Schwiedrzick et al. [66] which was available as a user defined material for Abaqus (UMAT) and explained in more detail in the following section. The same young's modulus and poisson's ratio was used in the proximal cortex, modeled as a linear elastic, isotropic material.
Trabecular bone was also modeled as a constant linear-elastic, isotropic material. The Young's modulus was chosen according to Synek et al. [67].
The implant was made out of titanium alloy TiAl6VA, therefore the Young's modulus was 114 GPa and a poisson's ratio of 0.3434 [68]. The yield limit was assumed to be 830 MPa.

	Material model	**Symmetry**	**E[MPa]**	$\nu[-]$
Proximal cortex	Linear-elastic	Isotropic	19327	0.3434
Distal cortex	Visco-plastic, damage	Isotropic	19327	0.3434
Trabecular bone	Linear-elastic	Isotropic	1400	0.3
Implant	Elasto-Plastic	Isotropic	114000	0.3

Table 2.3: Overview of the material modelling approach

The distal cortex was modeled as nonlinear material as proposed by Schwiedrzick et al. [66]. In this study, isotropy and a constant density of 1 was assumed for cortical bone. The resulting material parameters are displayed in Table 2.4. For more details on the material model, the reader is referred to Schwiedrzick et al. [66].

E_0 [MPa]	$\nu_\mathbf{0}$ [-]	$\sigma_\mathbf{0}^+$ [MPa]	$\sigma_\mathbf{0}^-$ [MPa]	ζ_0 [-]
19327	0.3434	144.7	234.2	0.49

Table 2.4: Yield material constants of the distal cortical bone

E_0 denotes the Young's modulus, $\nu_\mathbf{0}$ the poisons ratio, $\sigma_\mathbf{0}^+$ the uniaxial tensile yield stress, $\sigma_\mathbf{0}^-$ the uniaxial compressive yield stress, ζ_0 the biaxial interaction parameter in table 2.4.

The interfaces between parts were defined with physiological conditions in mind. Figure 2.12 shows where the interfaces are located, where as Table 2.5 gives an overview of

the interface type. The interfaces of the post-implantation reference model are discussed in this chapter, the other models are discussed in Chapter 2.3 Model variation.

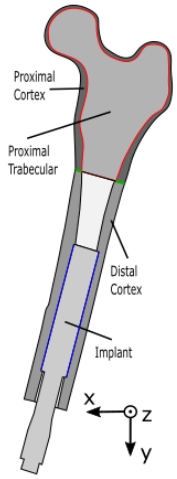

Figure 2.12: Location of interfaces in the post-implantation reference model

First Component	Second Component	Colour in Fig. 2.12	Interface Type
Proximal cortex	Proximal trabecular	Red	Tied
Proximal cortex	Distal cortex	Green	Tied
Distal cortex	Implant	Blue	Friction

Table 2.5: Modelling of the material interfaces

For the tied constraints the rotational and translational degrees of freedom (DoF) were constrained on the respective surfaces. The frictional interface was defined as a surface to surface contact, with a friction coefficient of 0.6, a slip rate of 0.05 and a hard contact (Table 2.6). The friction coefficient and slip rate were based on [69, 70].

	Friction coefficiant	Slip rate	Pressure-overclosure
Tangential behavior	0.6	0.05	-
Normal behavior	-	-	Hard Contact

Table 2.6: Parameters of the interfaces

The boundary conditions (BC) of the model were imposed with physiological conditions in mind. First the bone was tilted by 15° around the anterior-posterior axis (adduction), according to in vivo measurements from Orthoload [71] as well as Bergmann et al. [72]. Figure 2.13 gives an overview of the BC that were imposed.
The distal part of the implant is constrained in all spatial directions (6 DoF). Additionally a reference node was generated in the center of the femur head, which was kinematically coupled with 6 DoF to the outer nodes of the femur head.

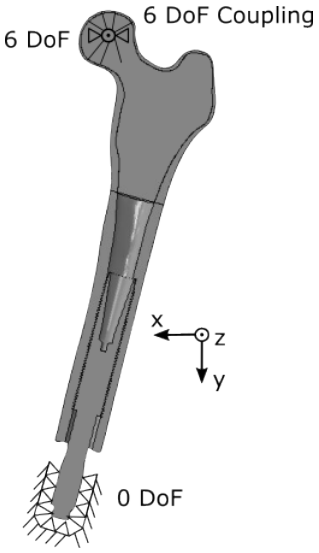

Figure 2.13: Boundary conditions of the finite element model

2.2.3 FE Model Solving and Postprocessing

A displacement of 7mm was applied in y-direction on the reference node. This magnitude was chosen to ensure that the failure load was reached and surpassed. Geometrical non-linearities were enabled to account for large displacements. The output variables were loads and displacements on the nodes, stresses and strains of the elements and solution dependent state variables such as the bones scalar damage variable D, where 0 denotes the fully undamaged state and 1 is fully damaged (see chapter 2.2.2). The latter were defined as part of the Schwiedrzick et al. model [66]. Post-processing was done at a physiological and ultimate load. The respective physiological load is 700N. This value is based on the resultant single stance force of 93% bodyweight measured by Frossard et. al. [38] and the assumption that an average male weighs 75kg. The ultimate load is defined as the highest load of the respective model.

Micromotion was evaluated in the course of the postprocessing and defined as the relative motion at the implant-bone interface under physiological load. Large relative interfacial motion, may result in loosening or failure of the implant, due to reduced osseointegration [73].
In this study, the micromotion calculation was based on the paper of Levadnyi et al. [74], additionally Figure 2.14 explains the calculation graphically. First the coordinates in the undeformed state as well as the coordinates under physiological load of every node on the bone-implant interface were returned. A custom python script, matched the bone-nodes to the implant-nodes according to their coordinates before the load was applied. The physiological load coordinates of the matching nodes were returned and the micromotion computed with following formulae:

$$m_j = \sqrt{(x_{\mathrm{i},j} - x_{\mathrm{b},j})^2 + (y_{\mathrm{i},j} - y_{\mathrm{b},j})^2 + (z_{\mathrm{i},j} - z_{\mathrm{b},j})^2} \tag{2}$$

Where m_j denotes the micromotion at node j, $x_{\mathrm{i},j}$ the implants x-coordinate at physiological load for node j and $x_{\mathrm{b},j}$ the bones x-coordinate at physiological load for node j (the y and z coordinate are noted analog).

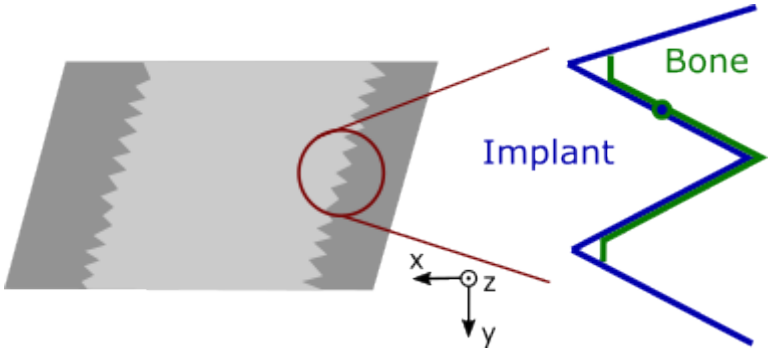

Figure 2.14: Schematic outline for the micromotion calculation

2.2.4 Mesh Convergence

As previously stated the finite element method is an approximate solution of a complex model, by splitting it into smaller sub-parts. The fewer sub-parts included in the model, the higher the potential error in the solution, therefore the number of elements (sub-parts) is increased creating a fine mesh. The major limitation is the computational time needed to solve a finely meshed model. Thus finding the balance between accuracy and computational time is of great importance. This is achieved with a mesh convergence study. The subsequent chapter gives an overview of the two mesh convergence studies performed as part of this thesis which were performed on the reference model simulating the post-implantation state (e.g., with contact interface).

First the full model convergence was analyzed in terms of ultimate load . A very coarse first order mesh was used, this was gradually made finer until the solution converged. The calculation was also repeated with a second order mesh, confirming the error does not increase greatly. In Figure 2.15 the ultimate load was plotted over the number of elements. The grey line shows the first order calculation, the red dot the second order. The first order calculation converged and therefore a total number of 1,716,861 (Seed size 1.1) nodes (green dot) was chosen for the model.
The error between the model with the highest and lowest number of elements is less than five %, indicating that the prediction of the ultimate load is fairly robust with respect to the number of elements used.

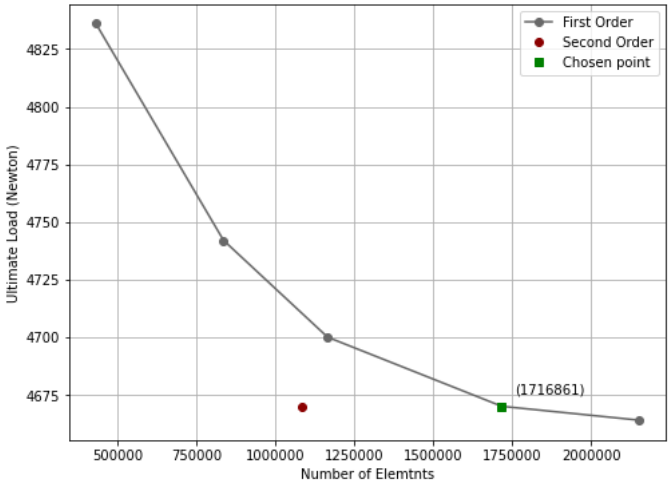

Figure 2.15: The mesh convergence of the full model evaluated by the ultimate load at different number of elements

Second, a sub-model was evaluated for which the most critical slice of the model was removed - the proximal end of the implant (Figure 2.16). This slice was modeled similar to the global model, the same materials and interfaces were applied. A displacement of 7mm was placed on a reference node, that was kinematically coupled to the most proximal surface of the bone. The most distal surface of the implant was constrained in all DoF.

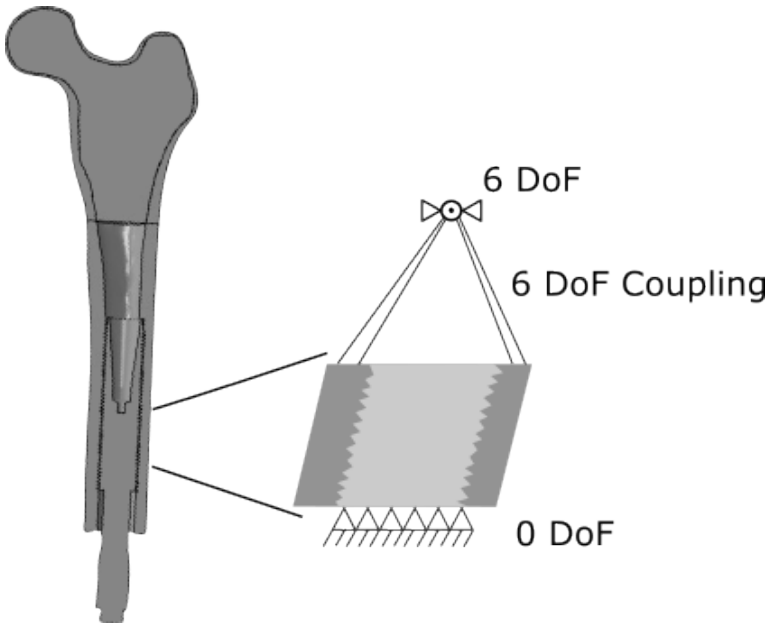

Figure 2.16: Finite element sub-model for mesh convergence study

As previously, the study was started with a coarse first order mesh, which was made finer until the solution converged (Grey Line in Fig. 2.17). The calculation was again done with a second order mesh (red dot), additionally the mesh coarseness chosen in the first mesh convergence study is highlighted with a green square.

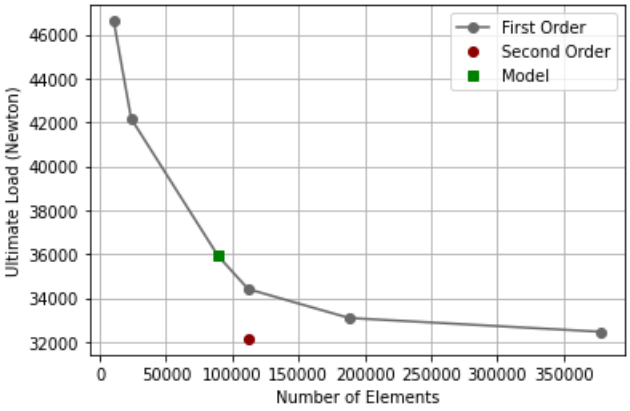

Figure 2.17: The mesh convergence of the sub-model evaluated by the ultimate load at different number of elements

The error between the first and second order calculation, evaluated at 112,046 nodes was 7.01%.

Furthermore, the micromotion for a coarse (89,386 nodes) and fine (378,316 nodes) mesh were evaluated at a physiological load of 700N. Figure 2.18 shows the mean and standard deviation of both. The error between the calculated means amounted to 4.91%.

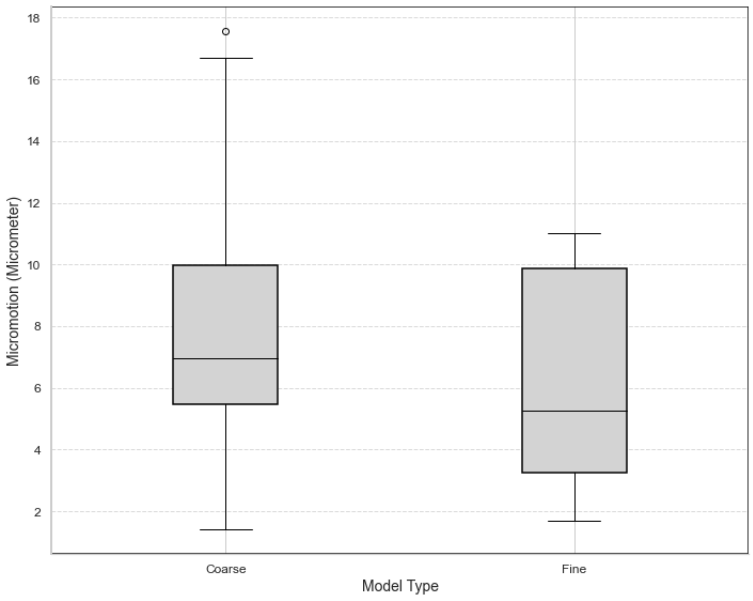

Figure 2.18: Micromotion evaluated at a coarse (89,386 nodes) and fine (378,316) mesh of the sub-model

The error in the micromotion is acceptable, as the mean micromotion is below five percent. Since the error in the ultimate load and the error of the mean micromotion was below five %, the chosen meshing parameters were considered acceptable.

2.3 Model Variation

The study included the evaluation of biomechanical behavior, using different model variations. The red path in Figure 2.19 highlights the reference model, discussed in the previous chapters. The biomechanical behaviour post-implantation and osseointegration (A) and model simplifications (B) are discussed in the subsequent chapter.

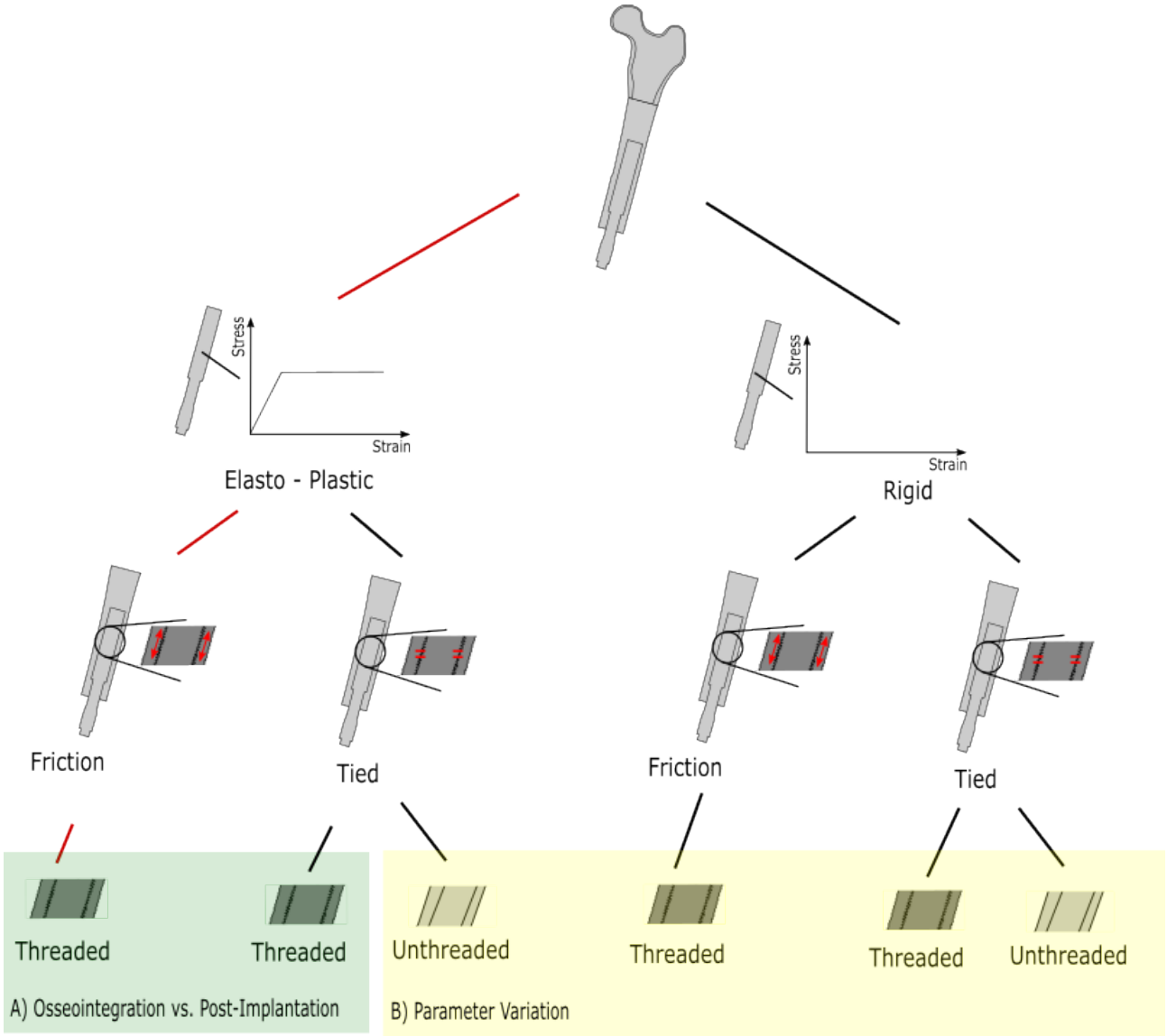

Figure 2.19: Outline of the different models and changed parameters

2.3.1 Post-Implantation vs. Osseointegration

The overall mechanical stability can be divided into post-implantation, often referred to as primary stability and osseointegration, or secondary stability. The former is defined at the time of implantation and is related to the contact condition between the implant and bone [75, 76, 77, 78]. After the biological process of healing, modeling of bone and improved load transfer, the implant is considered osseointegrated [79, 80].

In this study the post-implantation is modeled with a friction interface between the distal cortex and implant (Chapter 2.2.2). In an additional model the contact was changed to a tie constraint for the translational and rotational DoF at the bone-implant interface, representing perfect osseointegration.

2.3.2 Parameter Study

The goal of the parameter study was to test how simple the model can be designed, while still capturing the biomechanical behaviour of the reference model. For this, the implant material was changed from elasto-plastic to rigid, simplifying the material model. This material model was used for post-implantation, using the friction contact (Chapter 2.2.2) as well as osseointegration, with the tied constraint between the distal cortex and implant (Chapter 2.3.1). Further simplifications were done with the bone-implant interface by removing the threading. This was achieved by removing the thread from the implant geometry and performing all steps as mentioned in Chapter 2.2.1 with the unthreaded implant. The thread was straightened at the pitch diameter (Figure 2.20), since the pitch (P) and height (H) of the thread is exactly the half at this diameter.

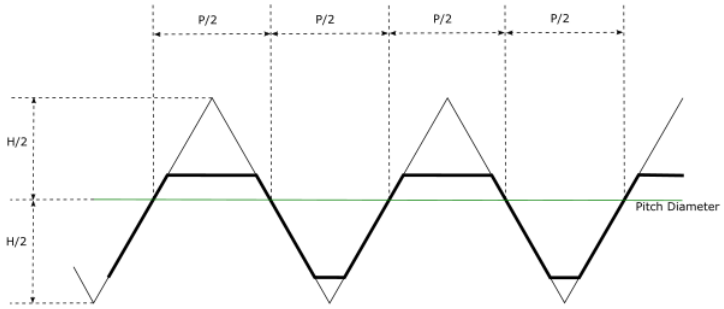

Figure 2.20: Geometry of the axial implant thread, with the most important dimensions, the pitch (P) and height (H)

3 Results

The results are structured to firstly present the reference model and then compare the chosen models, to the reference. The sections are structured into a Load-displacement graph, followed by the evaluation at physiological as well as ultimate load. The scale factor of the finite element graphs, if not mentioned otherwise, is one.

3.1 Reference Model

In this section the reference model is presented. It has an elasto-plastic threaded implant, which is modeled with a friction constraint between bone and implant. Figure 3.1 shows the load-displacement curve, additionally the physiological and ultimate load, at which the deformations, stresses, damage, and micromotion will be compared, are displayed with the dashed lines.

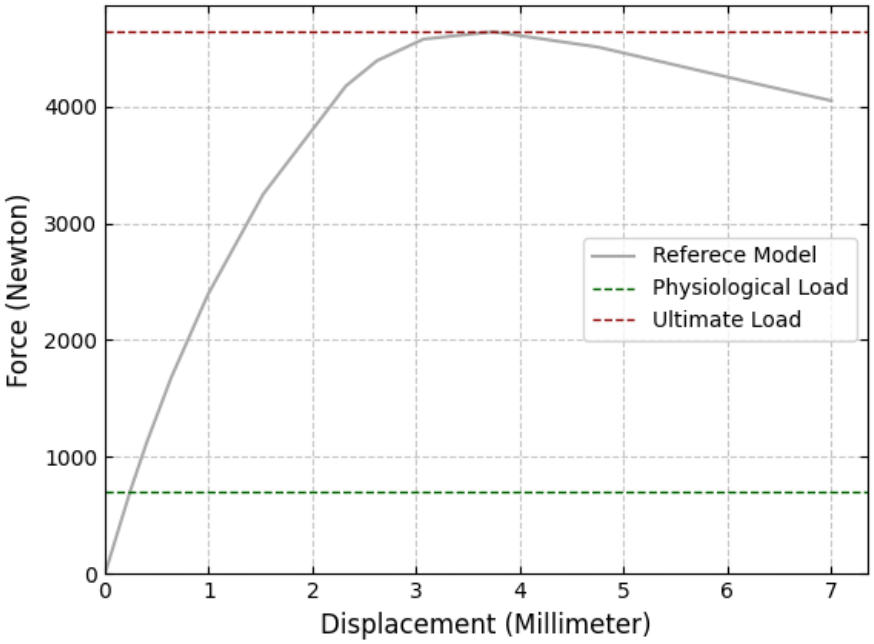

Figure 3.1: Load-displacement curve of reference model, showing the physiological load and ultimate load

The physiological load, was defined as 700N, which as mentioned in section 2, is the average weight of a male. The ultimate load of the reference model had a magnitude of 4.6kN.

3.1.1 Physiological Load

Figure 3.2 shows the deformation in lateral and anterior view (a) and the von Mises stress in lateral view with a coronal cut (b) at physiological load. In figure 3.2(c) the maximum limit of the colour map was reduced by 90%, from 100 MPa to 10 MPa, to make the stresses in the bone visible.

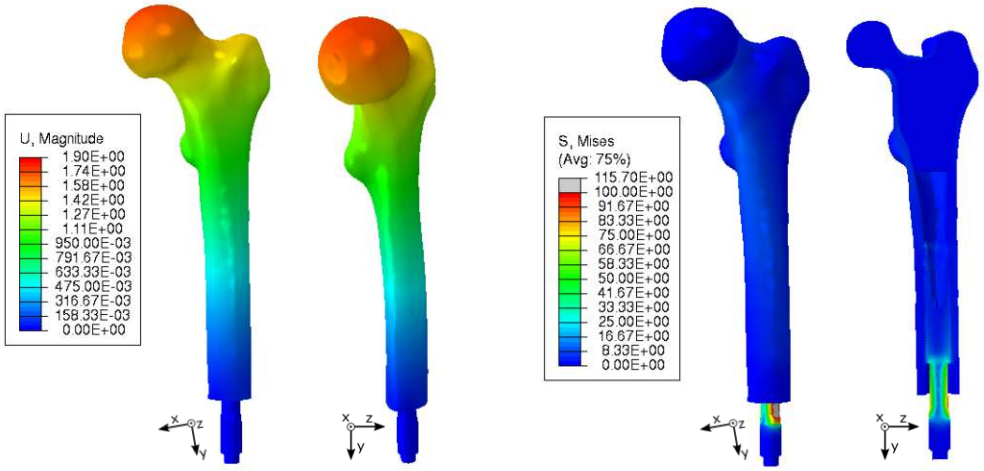

(a) Deformation

(b) Stress

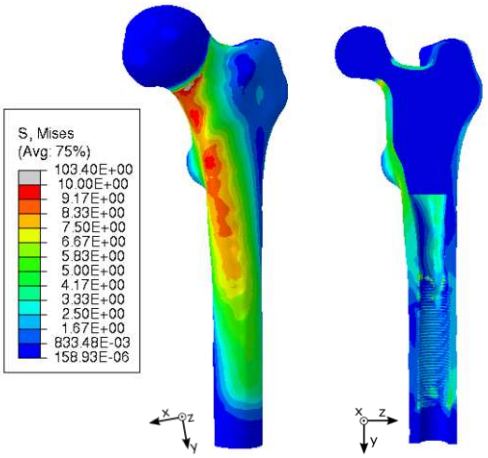

(c) Stress in bone

Figure 3.2: Finite element plots of the reference model at physiological load

A slight deformation at physiological load can be observed. The maximum deformation of 1.8 mm occurs in the proximal part of the femur, the head. Further distal in the bone, the magnitude reduces to zero at the abutment screw, as the implant is fixed in this position. The largest von Mises stresses were observed in the implant system at the abutment screw, these stresses ranged up to 116 MPa. The highest stress can be seen laterally on the implant.
The highest stress in the bone is located in the cortex around the femoral neck and shaft. The threads in the bone show approximately 3 MPa, compared to the 10 MPa in the femoral neck.

Figure 3.3 shows a box plot of the micromotion.

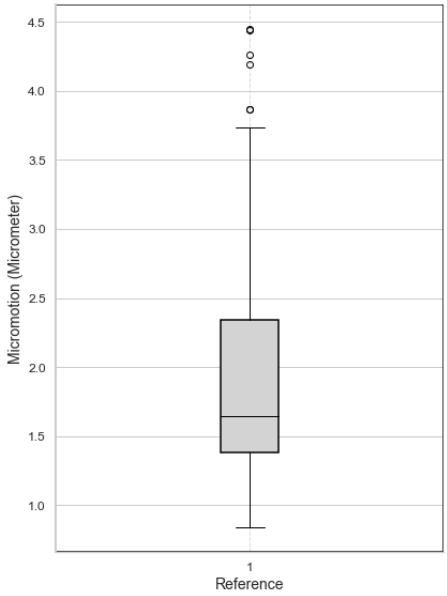

Figure 3.3: Micromotion of the reference model shown as a boxplot

The mean micromotion is 1.5 μm, the maximum value is 4.5 μm and the minimum value is 0.8 μm.

3.1.2 Ultimate Load

Figure 3.4 shows the deformation in lateral and anterior view (a) and the von Mises stress in lateral view with a coronal cut (b) at ultimate load. In figure 3.4(c) the maximum limit of the colour map was reduced by 91%, from 1000 MPa to 90 MPa, to make the stresses in the bone visible.

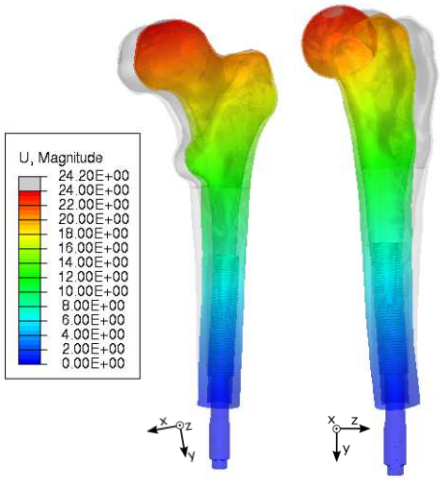

(a) Deformation

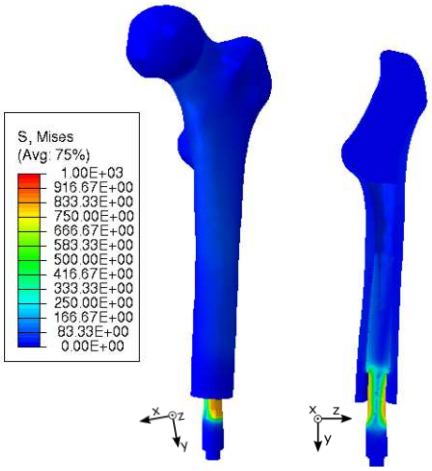

(b) Stress

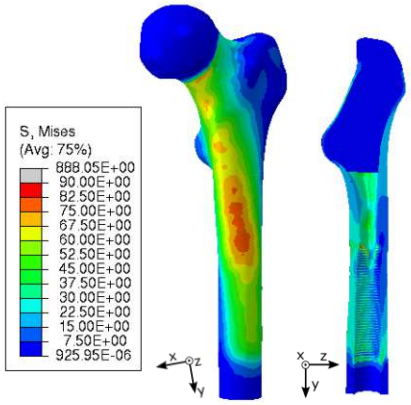

(c) Stress in bone

Figure 3.4: Finite element plots of the reference model at ultimate load

The unloaded bone is shown half-transparent to make the deformation visible. The bone deforms in lateral, posterior and proximal direction. The displacement at ultimate load is 24.2 mm.
Similar to the physiological load case, the largest von Mises stress is located at the stem of the implant ranging up to 888 MPa, at which point the implant has yielded. Similar to the physiological load higher stresses can be seen lateral in the abutment.
The highest stress in the bone is again visible in the femoral neck and shaft, the trabecular bone inside the proximal femur shows no significant stress peaks. The threads show some stress, but the highest stresses were found in the femoral shaft.

Figure 3.5 shows the scalar damage variable of the reference model in posterior view with a coronal cut. On the right of the figure, the most damaged areas are shown in more detail.

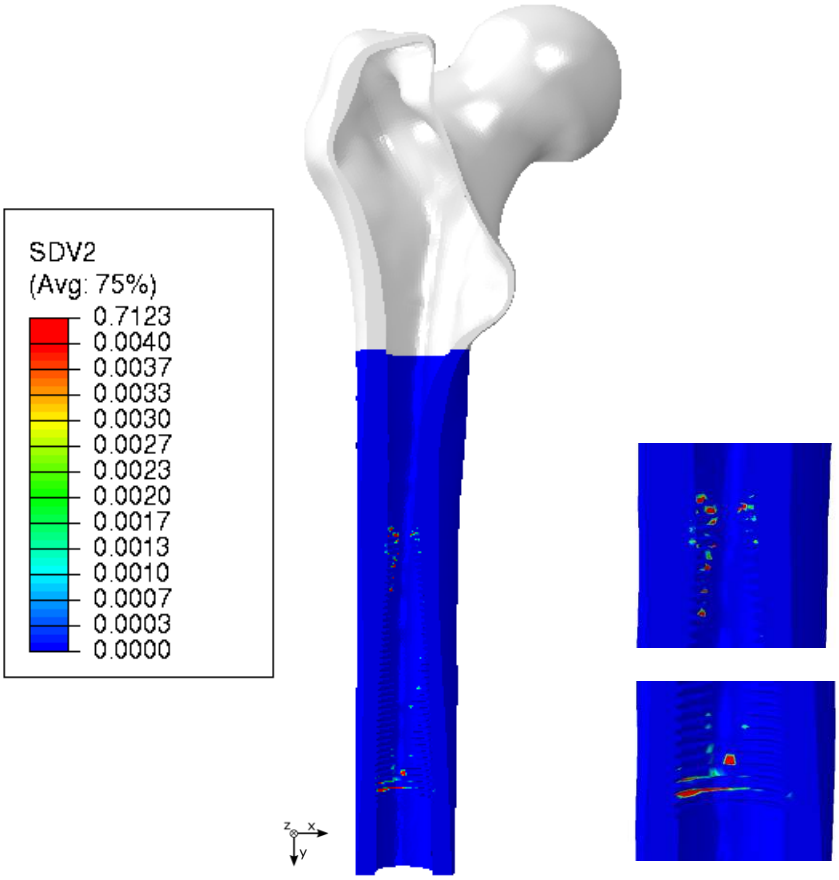

Figure 3.5: Bone damage of reference model at ultimate load

However, the damage variable D had a value below 0.004, only a few elements exceed that value, they can therefore be considered as artefacts. The biggest damage is located in the last few threads, at the most proximal and distal part of the bone. The damage is located more lateral within the femur.

3.2 Reference Model - Post-Implantation vs. Osseointegrated

In this section the post-implantation reference model, discussed in the previous chapter 3.1 will be compared to the osseointegrated reference model. The differentiation between the models being the bone-implant interface constraint, which is tied for the osseointegrated model and frictional for the post-implantation model. Figure 3.6 shows the load-displacement curves of both models.

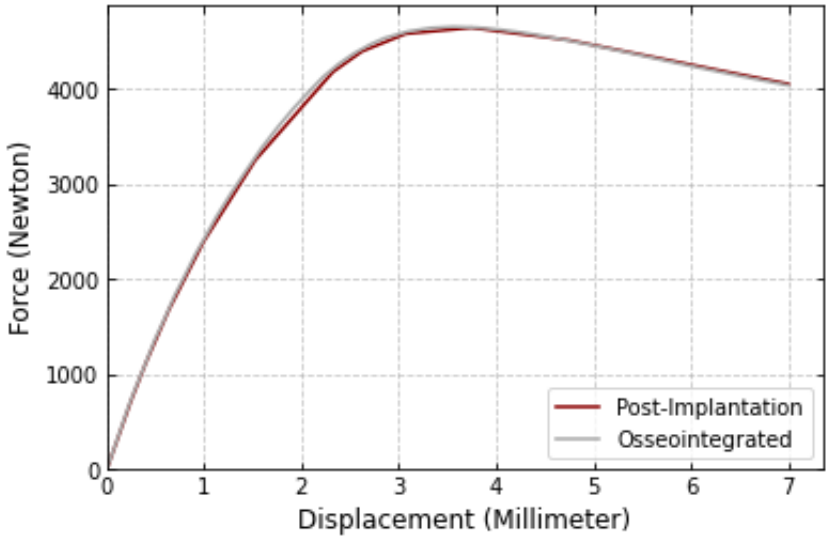

Figure 3.6: Load-displacement curve of the reference model - post-implantation vs. osseointegrated

No notable difference between the models can be detected. The ultimate load of the reference model occurred at a displacement of 3.7mm with a magnitude 4.6kN. Whereas the ultimate load of the osseointegrated model occurred at a displacement of 3.6mm with a magnitude 4.6kN.

3.2.1 Physiological Load

Figures 3.7 and 3.8 show the deformation and von Mises stress at physiological load in anterior and lateral view.

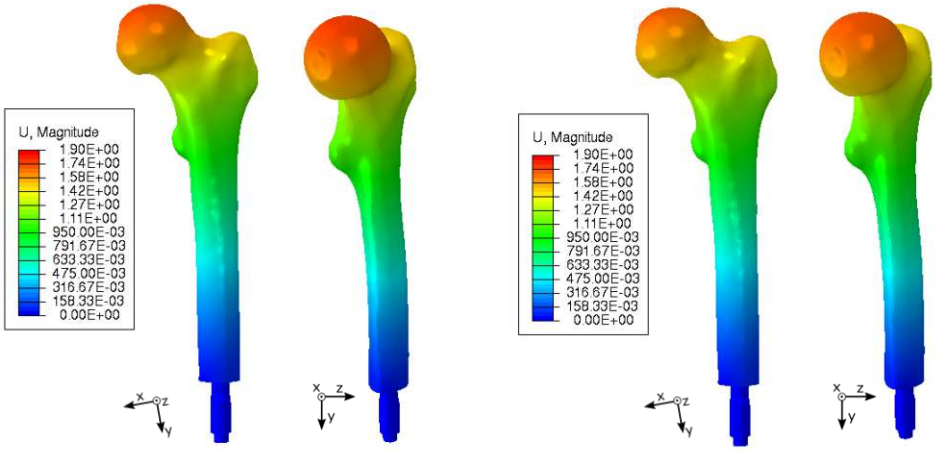

(a) Post-Implantation (b) Osseointegrated

Figure 3.7: Deformation at physiological load of the reference model - post-implantation vs. osseointegrated

The osseointegrated model, when compared to the post-implantation model, showed approximately six percent less maximum displacement magnitude. The slight difference is visible proximal of the great trochanter, distally no difference can be observed.

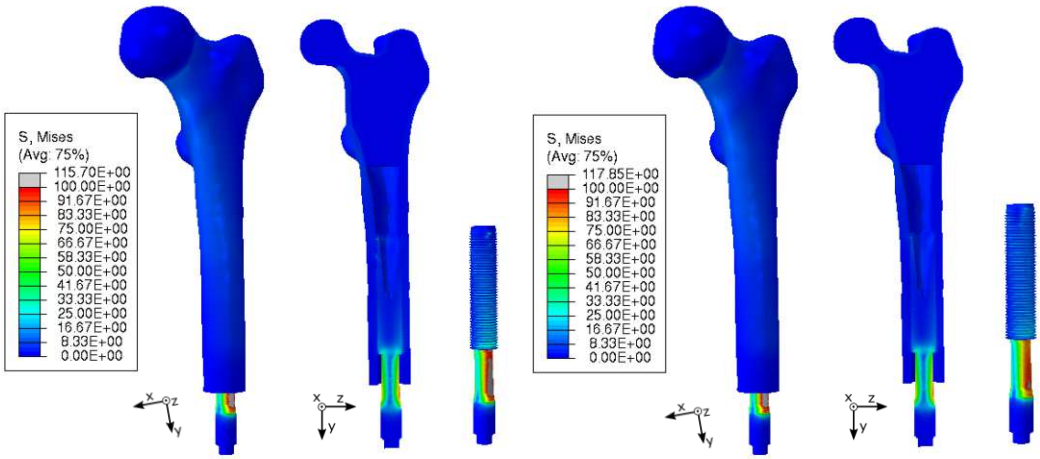

(a) Post-Implantation (b) Osseointegrated

Figure 3.8: Stress at physiological load of the reference model - post-implantation vs. osseointegrated

The osseointegrated model, when compared to the post-implantation model, shows approximately two percent higher peak von Mises stress. The highest stress can be observed distally, in the abutment. The stress distribution in the coronal cut of the implant is

similar between the models. The detailed view of the implant, highlights a difference on the lateral side proximal of the abutment screw, a larger area surpassing 100 MPa can be observed.

Figure 3.9 shows the stress in the bone by reducing the colour map by 90%.

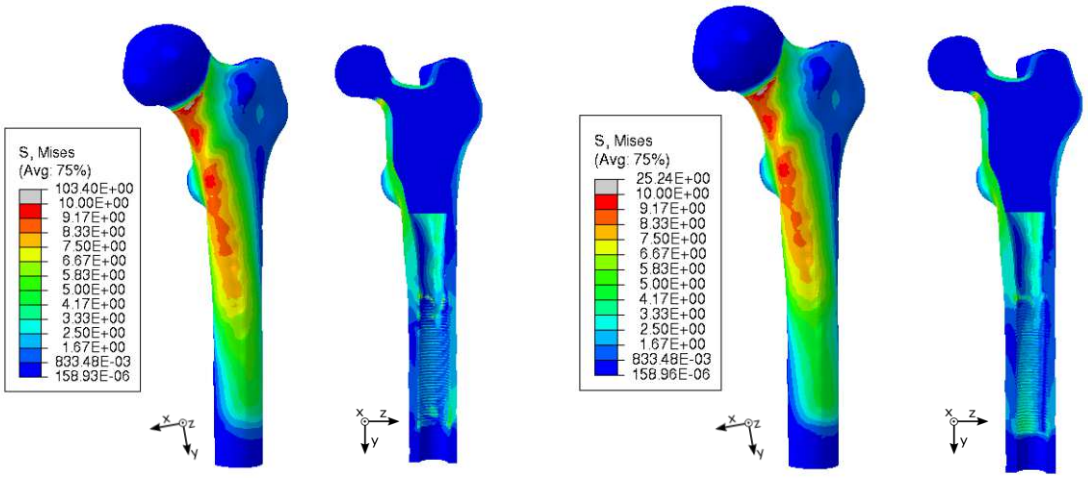

(a) Post-Implantation (b) Osseointegrated

Figure 3.9: Bone deformation at physiological load of the reference model - post-implantation vs. osseointegrated

A similar stress distribution between the models can be seen, even though the maximum value of the post implantation model is 75% higher. In the osseointegrated model, the threads in the bone show slightly less severe stress jumps.

3.2.2 Ultimate Load

Figures 3.10 and 3.11 show the deformation and von Mises stress at ultimate load in anterior and lateral view.

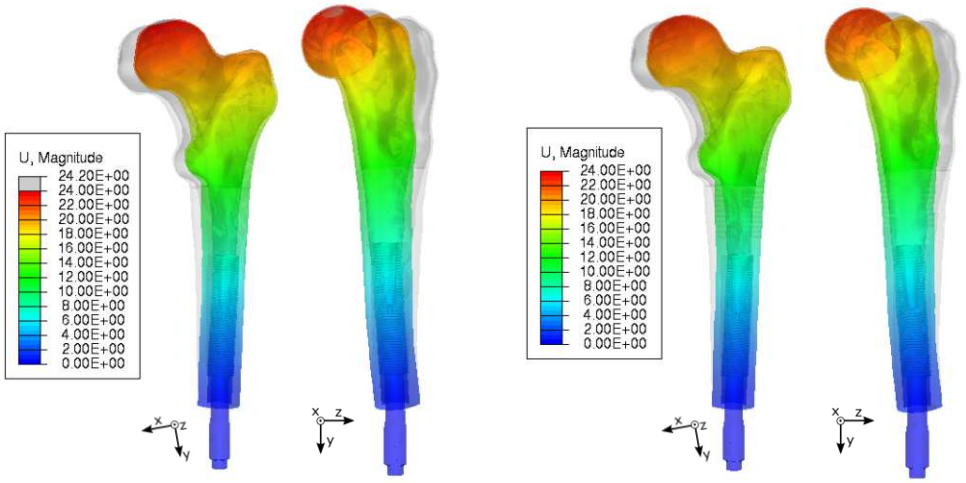

(a) Post-Implantation (b) Osseointegrated

Figure 3.10: Deformation at ultimate load of the reference model - post-implantation vs. osseointegrated

The post-implantation and osseointegrated model, both deformed in lateral, posterior and proximal direction. The difference in deformation magnitude is approximately one percent and no visible differences in the stress distribution can be seen.

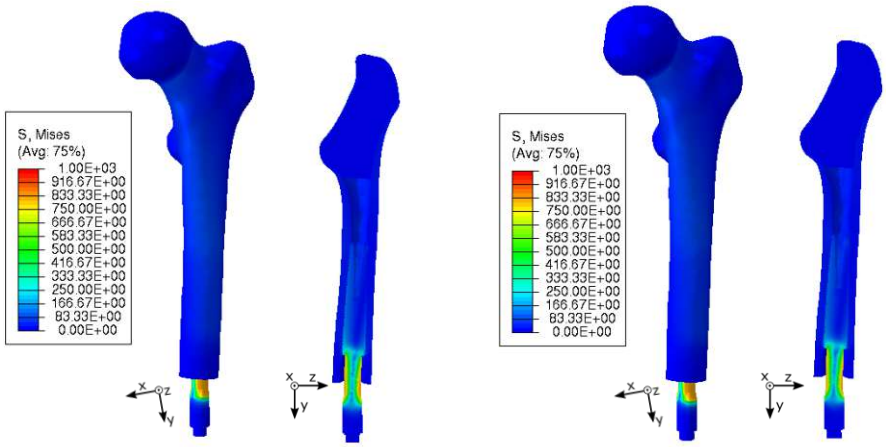

(a) Post-Implantation (b) Osseointegrated

Figure 3.11: Stress at ultimate load of the reference model - post-implantation vs. osseointegrated

The highest von Mises Stress of both the post-implantation and osseointegrated model, is located at the stem of the implant. There is no visible difference between the values as well as stress distribution, when comparing the models. Higher stress can be seen lateral in the abutment, which yields in both models.

Figure 3.12 shows the stress within the bone, by scaling the colour map. The maximum value displayed in colour is 90 MPa, compared the 1000 MPa in Figure 3.10.

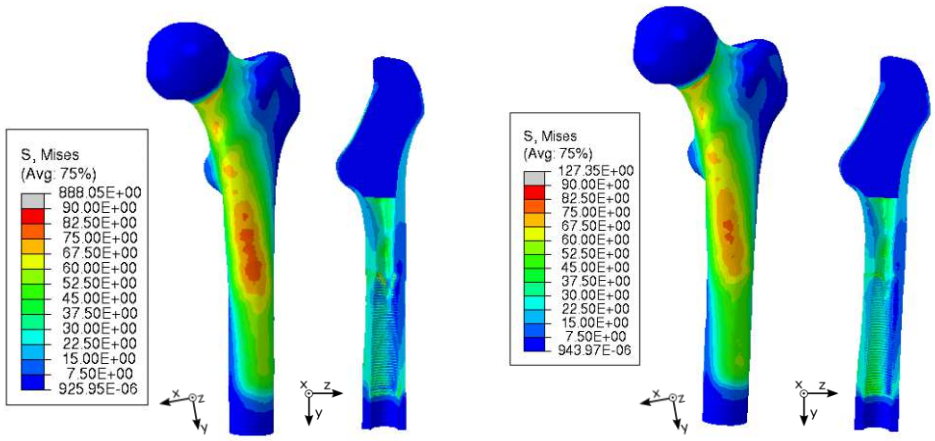

(a) Post-Implantation (b) Osseointegrated

Figure 3.12: Bone Stress at ultimate load of the reference model - post-implantation vs. osseointegrated

The location of the von Mises stress is comparable between the models, the highest stress can be observed in the femoral shaft and neck. The post implantation model shows slightly higher stress around the region at which yielding of the implant starts. As previously mentioned, the threads of the osseointegrated model have a more continuous stress distribution.

Figure 3.13 shows the damage plot in posterior view with a coronal cut.

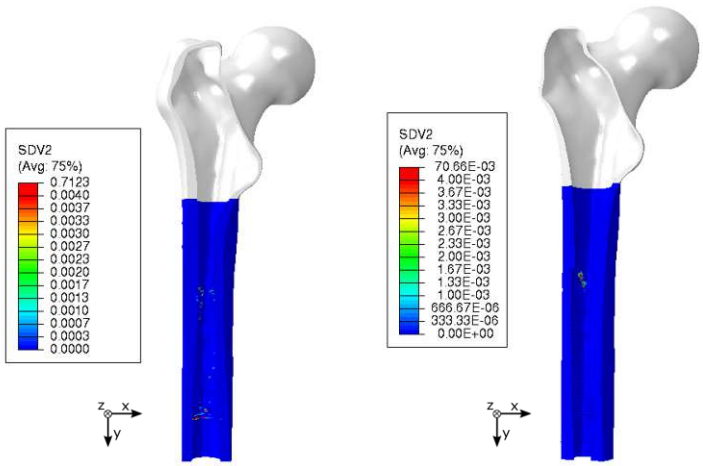

(a) Post-Implantation (b) Osseointegrated

Figure 3.13: Bone damage of the reference model - post-implantation vs. osseointegrated

No substantial damage can be observed in either model. The post-implantation model shows damage distributed at the proximal and distal end of the implant, whereas the osseointegrated damage is concentrated in one area on the proximal end.

3.3 Post-Implantation Model - Reference vs. Rigid

In this section the post-implantation reference model, discussed in chapter 3.1 will be compared to the rigid post-implantation model. The differentiation between the models being the implants material, one is elasto-plastic, whereas the other is modeled as a rigid. Figure 3.14 shows the load-displacement curve.

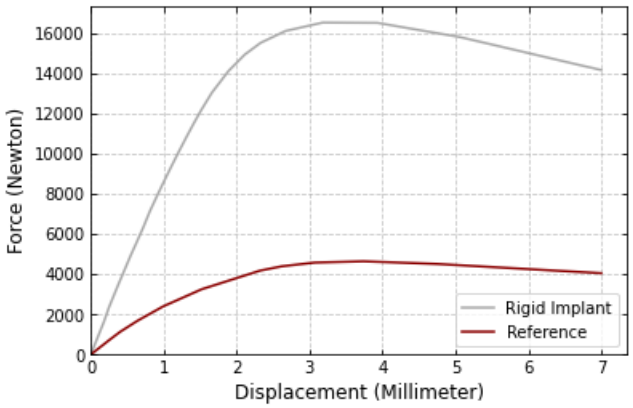

Figure 3.14: Load-displacement curve of the post implantation model - reference vs. rigid

The ultimate load of the reference model occurred at a displacement of 3.7mm with a magnitude 4.6kN. Where as the ultimate load of the model with a rigid implant occurred at a displacement of 3.2mm with a magnitude 16.5kN. The ultimate load increased by 259%.

3.3.1 Physiological Load

Figures 3.15 and 3.16 show the deformation and von Mises stress at physiological Load in anterior and lateral view.

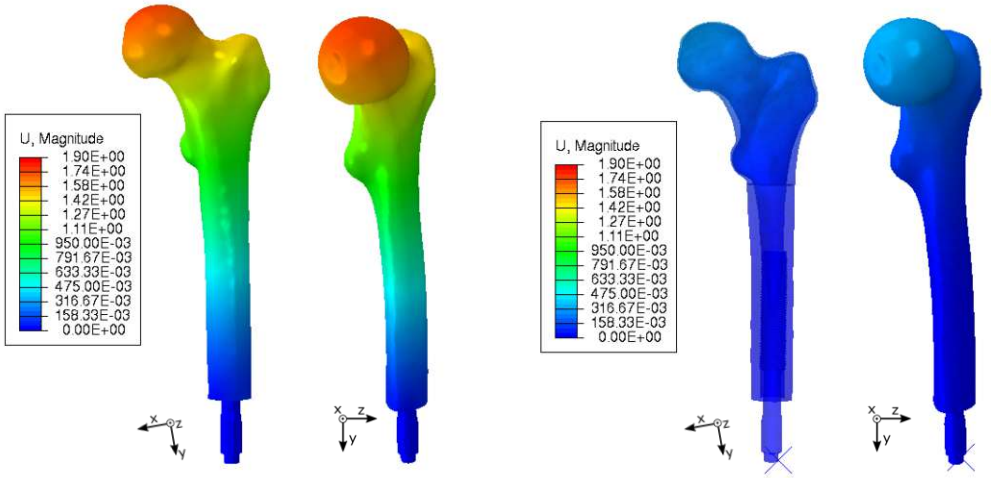

(a) Reference (c) Rigid

Figure 3.15: Deformation at physiological load of the post implantation model - reference vs. rigid

Compared to the reference, the rigid model deformed a lot less with the same load applied. A slight deformation of the rigid model is visible. Approximately 0.4 mm, compared to 1.9mm in the reference model, resulting in a aprox. 80% reduction. The rigid model only showed deformation in the femoral head and very slightly the neck, the shaft showed no deformation.

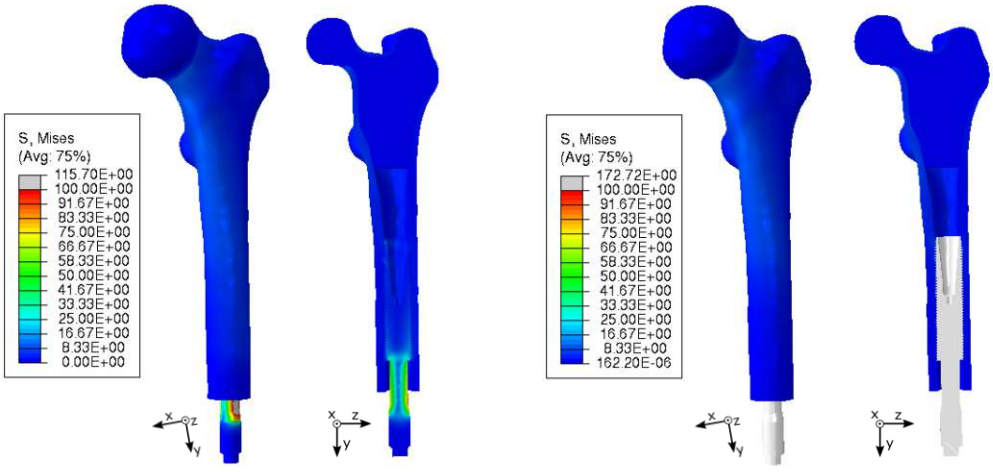

(a) Reference (b) Rigid

Figure 3.16: Stress at physiological load of the post implantation model - reference vs. rigid

As no von Mises stress can be calculated in a rigid material, only stresses in the bone are compared to each other. Figure 3.17, displays the bone stress by reducing the colour map scaling to 10 MPa.

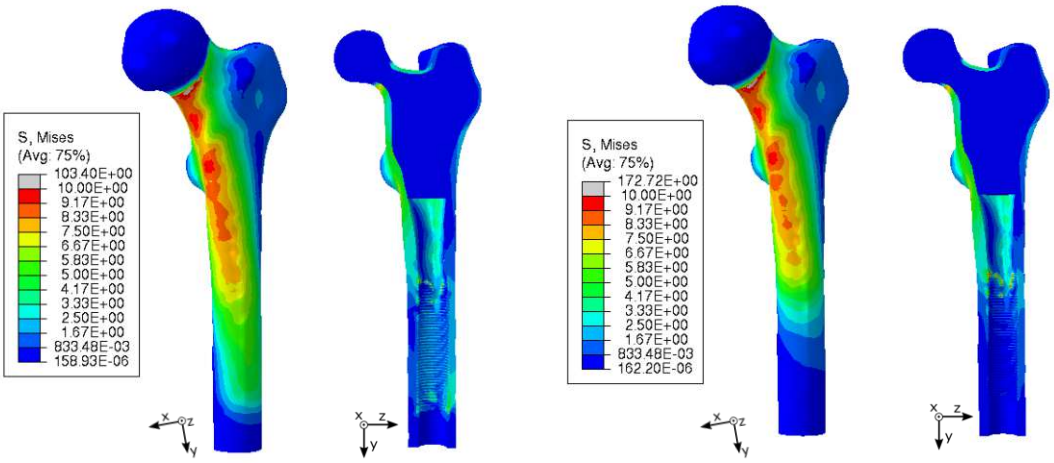

(a) Reference (b) Rigid

Figure 3.17: Bone stress at physiological load of the post implantation model - reference vs. rigid

The location of the highest stress in the rigid model is similar, to the reference model. Distally a difference can be seen, the rigid model shows low stress in the area where the implant is placed. Also the maximum stress values in the rigid model is increased by approximately 50%.

The following figure 3.18 shows a boxplot of the micromotion.

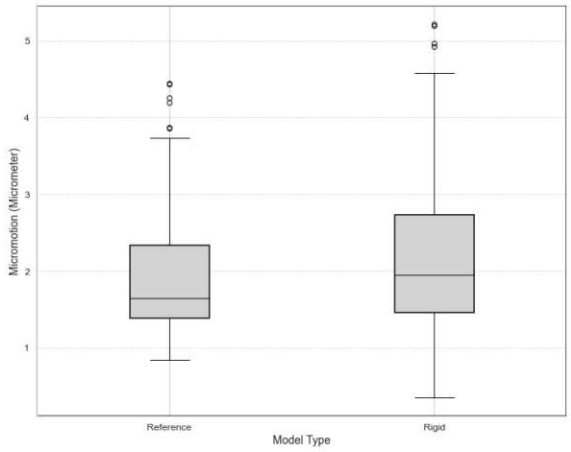

Figure 3.18: Post implantation micromotion shown in a boxplot - comparison of the reference vs. rigid model

The micromotion in the rigid model shows more variance compared to the reference model. The mean micromotion for the reference and rigid model hardly show a difference, for the former it is 1.5 μm and the latter 1.4 μm.

3.3.2 Ultimate Load

Figures 3.19 and 3.20 show the deformation and von Mises stress at ultimate load in anterior and lateral view.

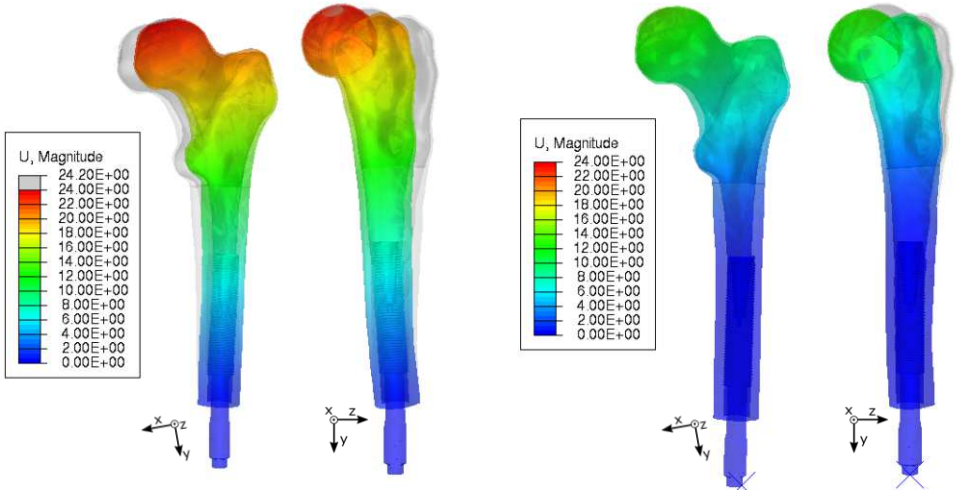

(a) Reference (c) Rigid

Figure 3.19: Deformation at ultimate load of the post implantation model - reference vs. rigid

The reference model, shows hardly any lateral and less proximal movement as the reference model. The rigid model, when compared to the reference has approximatly 67% less deformation. The difference is visible in the femur head, where the deformation is aprox. eight mm, compared to 24 mm in the reference model. The shaft of the rigid model shows no deformation in the area in which the implant is located.

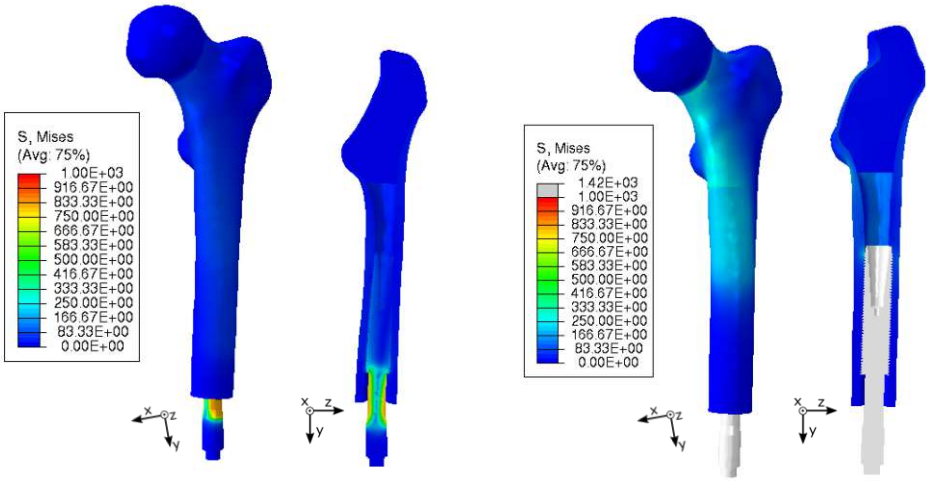

(a) Reference (c) Rigid

Figure 3.20: Stress at ultimate load of the post implantation model - reference vs. rigid

The largest von Mises stress on the rigid model is located at the femoral neck and medial femoral shaft, compared to the stem of the implant.

As no von Mises stress can be calculated in a rigid material, the bone rather than the implant stresses is compared to each other. Figure 3.21, displays the bone stress by reducing the colour map scaling to 90 MPa. This offers a comparison to the reference, in Figure 3.21(c) the colour map has been increased to 300 MPa to visualise the stress in the bone with more detail.

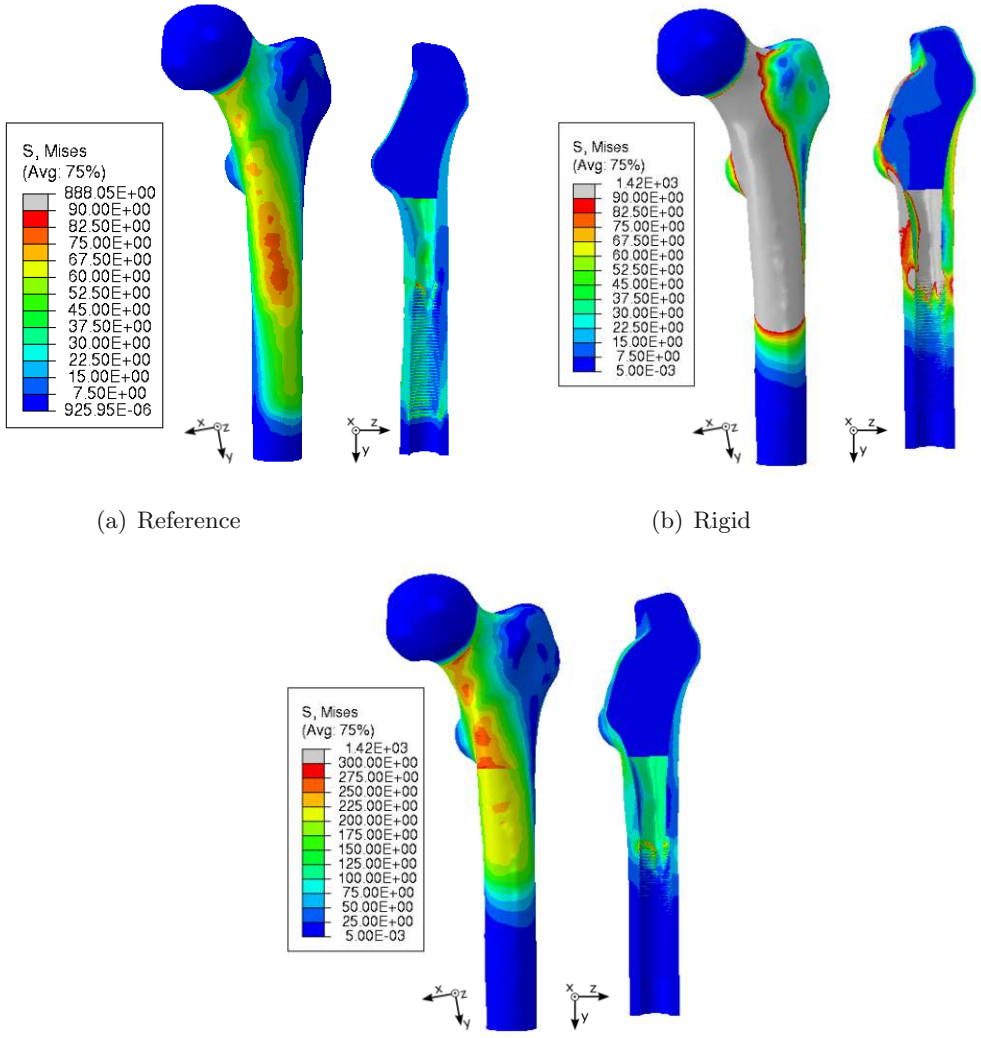

(a) Reference

(b) Rigid

(c) Rigid with adjusted colormap

Figure 3.21: Bone stresses at ultimate load of the post implantation model - reference vs. rigid

The highest stress distribution can be found in the femur neck and shaft, but as mentioned values above the average vary greatly. The reference model shows approximatly 90 MPa in the shaft, whereas the rigid model shows 300 MPa. Also distally, where the implant is located, the rigid model shows very low stress compared to the reference.
A jump in the stress between the distal and proximal part is clearly visible, suggesting that the bone damage occured near the interface of the distal and proximal parts, which are modeled as non-linear and linear materials, repectively. Thus, the results of the model

must be intepreted with caution at this load level.

Figure 3.22 shows the damage plot in posterior view with a coronal cut.

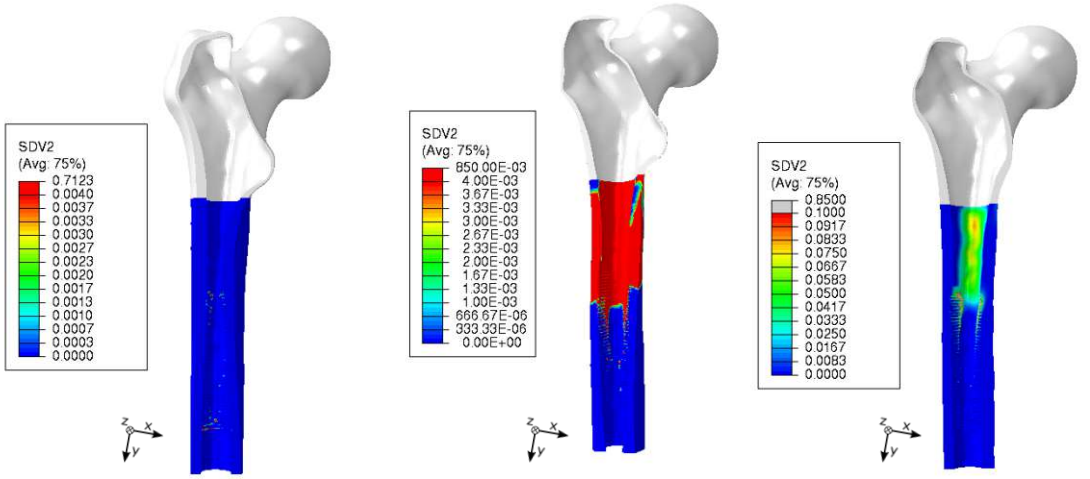

(a) Reference (b) Rigid (c) Rigid with adjusted colourmap

Figure 3.22: Bone damage (SDV2) at ultimate load of the post implantation model - reference vs. rigid

Subfigure (a) and (b) have the same colourmap range, allowing for comparison. The rigid model is clearly damaged alot more than the reference model, especially in the bone shaft, proximal of the implant. In subfigure (c) the colourmap limit was adjusted to visualise the bone damage of the rigid model in more detail. The most damage can be observed in the anterior part of the bone shaft, proximal of the implant. Approximately the first proximal third of the threads show damage in the medial and lateral bone shaft.
The damage of the rigid model is located in a different and much more extensive area.

3.4 Osseointegrated Model - Reference vs. Rigid

In this section the osseointegrated reference model will be compared to the rigid osseointegrated model. The differentiation between the models being the implants material properties, one is elasto-plastic, whereas the other is modeled as rigid. Figure 3.23 shows the Load-displacement curve.

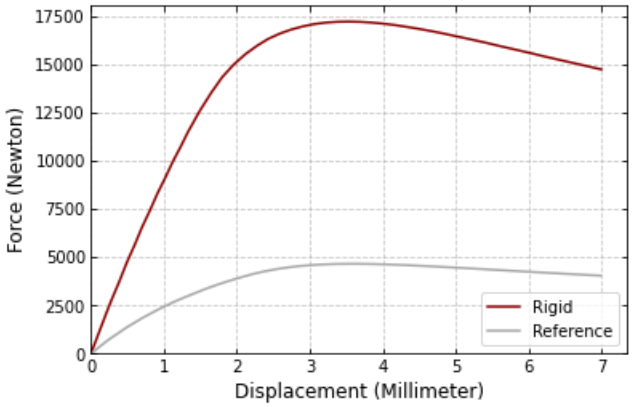

Figure 3.23: Load-displacement curve of the osseointegrated model - reference vs. rigid

The ultimate load of the reference model occurred at a displacement of 3.6mm with a magnitude 4.6kN. Where as the ultimate load of the model with a rigid implant occurred at a displacement of 3.5mm with a magnitude 17.2kN. The ultimate load increased by 274%.

3.4.1 Physiological Load

Figures 3.24 and 3.25 show the deformation and von Mises stress at physiological load in anterior and lateral view.

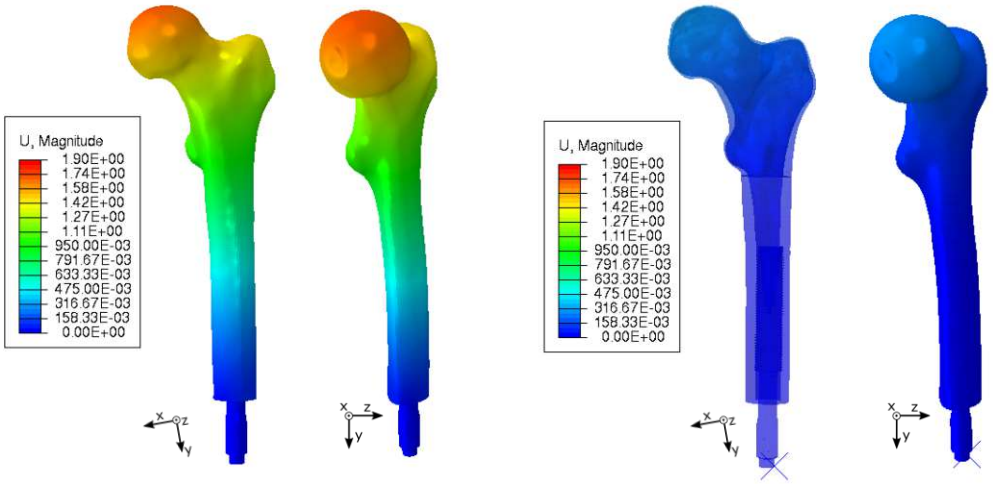

(a) Reference (b) Rigid

Figure 3.24: Deformation at physiological load of the osseointegrated model - reference vs. rigid

Compared to the reference, the rigid model deformed a lot less with the same load applied.

A slight deformation of the rigid model is visible. Approximately 0.4 mm, compared to 1.9mm in the reference model, resulting in a approx. 80% reduction. The rigid model only showed deformation in the femur head and very slightly in the neck. The bone shaft showed no deformation.

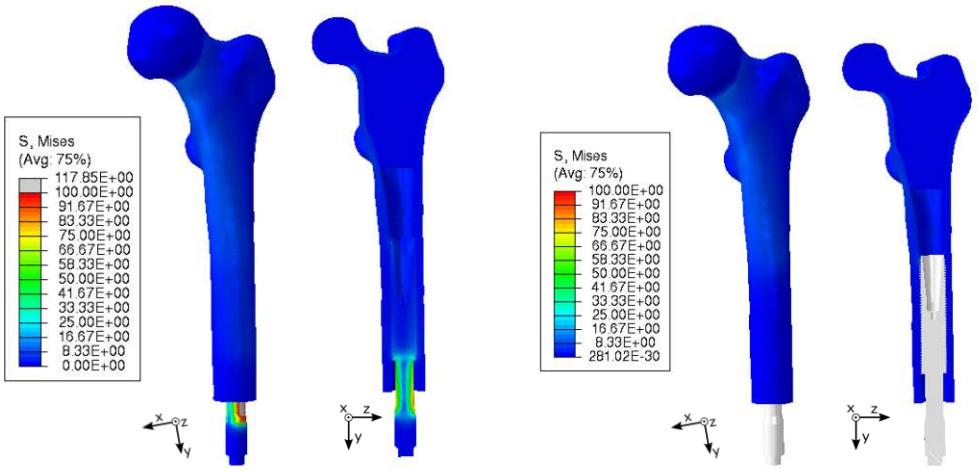

(a) Reference (b) Rigid

Figure 3.25: Stress at physiological load of the osseointegrated model - reference vs. rigid

No stress can be calculated in a rigid material, therefor only bone-stresses are compared.

Figure 3.26, displays the bone stress, by reducing the colour map range to 10 MPa.

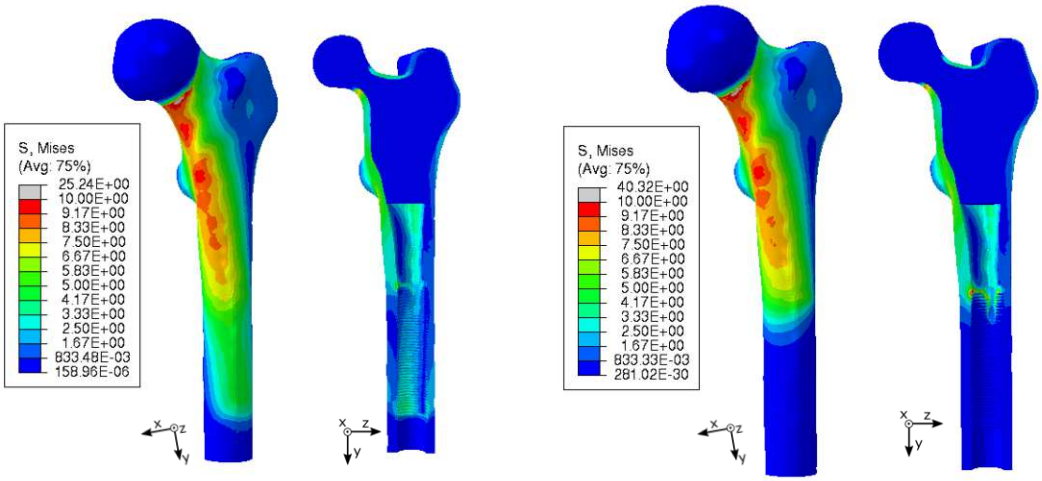

(a) Reference (b) Rigid

Figure 3.26: Bone stresses at physiological load of the osseointegrated model - reference vs. rigid

The location of the highest stress in the rigid model is similar, to the reference model. Distally a difference can be seen, the rigid model shows low stress in the area where the implant is placed. Also the maximum stress values in the rigid model is increased by approximately 60%.

3.4.2 Ultimate Load

Figures 3.27 and 3.28 show the deformation and von Mises stress at ultimate load in anterior and lateral view.

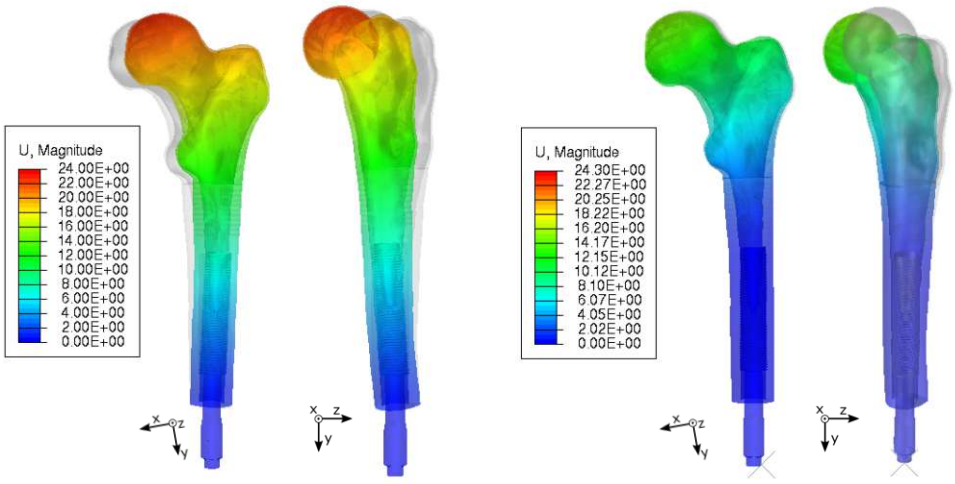

(a) Reference (b) Rigid

Figure 3.27: Deformation at ultimate load of the osseointegrated model - reference vs. rigid

The reference model, shows hardly any lateral and less proximal movement as the reference model. The rigid model, when compared to the reference has approximately 67% less deformation. The difference is visible in the femoral head, where the deformation is aprox. eight mm, compared to 24 mm in the reference model. The shaft of the rigid model shows no deformation in the area in which the implant is located.

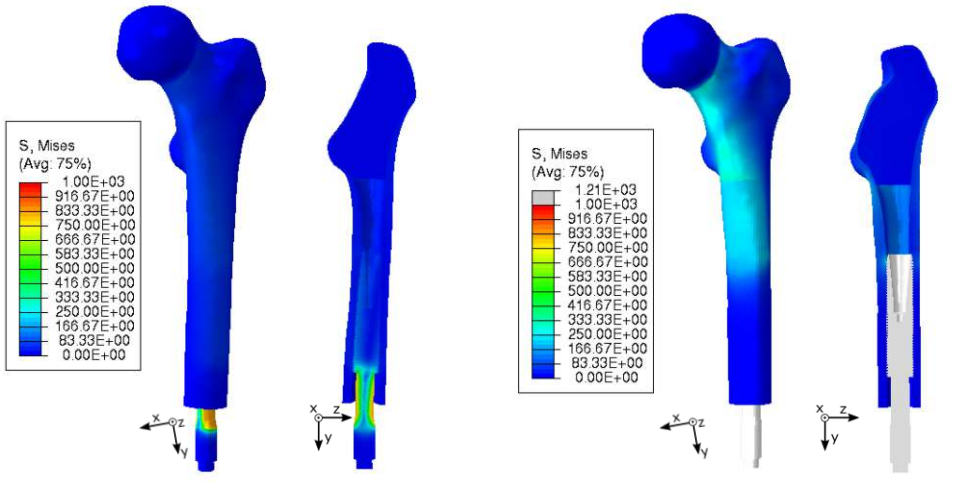

(a) Reference (b) Rigid

Figure 3.28: Stress at ultimate load of the osseointegrated model - reference vs. rigid

The largest von Mises stress in the rigid model is located on the femoral neck and medial shaft.

No von Mises stress can be calculated in a rigid material, therefor the bone rather than the implant stresses is compared to each other. Figure 3.29, displays the bone stress by reducing the colour map scaling to 90 MPa. This offers a comparison to the reference, in Figure 3.29(c) the colour map has been increased to 300 MPa to visualise the stress in the bone with more detail.

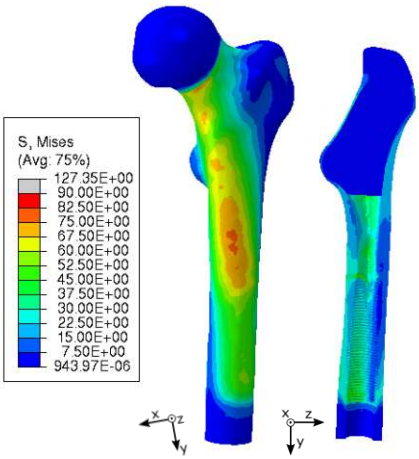

(a) Reference

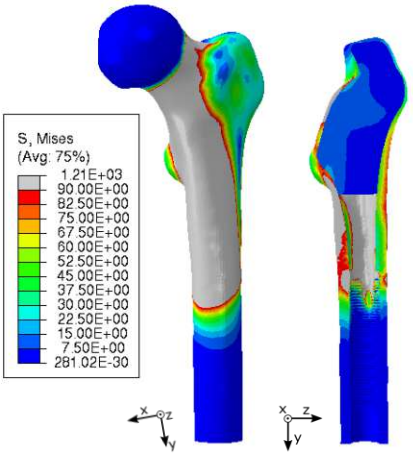

(b) Rigid

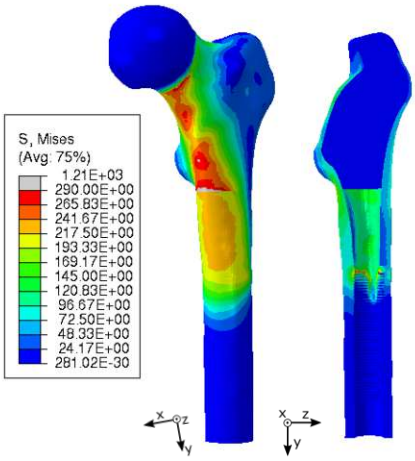

(c) Rigid - Adjusted colour map

Figure 3.29: Bone stresses at ultimate load of the osseointegrated model - reference vs. rigid

The highest stress distribution can be found in the femoral neck and shaft, but as mentioned above the average values vary greatly. The reference model shows approximatly 90 MPa in the shaft, whereas the rigid model shows 290 MPa. Also distally, where the implant is located the rigid model shows no stress compared to the reference. As mentioned previously a stress jump between the distal and proximal bone is visible, suggesting the results of the proximal bone are not reliable.

Figure 3.30 shows the damage plot in posterior view with a coronal cut.

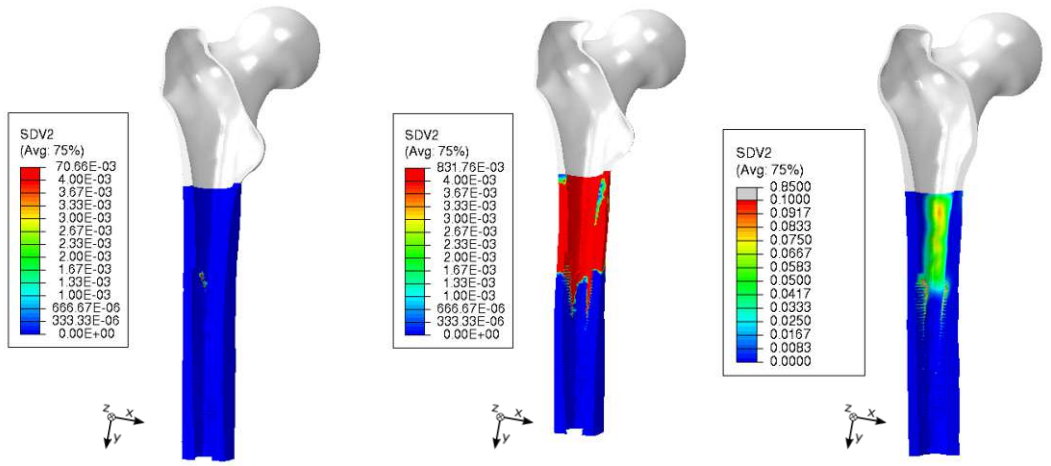

(a) Reference (b) Rigid (c) Rigid with increased colourmap

Figure 3.30: Bone damage at ultimate load of the osseointegrated model - reference vs. rigid

Subfigure (a) and (b) have the same colourmap limits, allowing for comparison. The rigid model is clearly damaged significantly more than the reference model, especially in the bone shaft, proximal of the implant. In subfigure (c) the colourmap limit was adjusted to visualise the bone damage of the rigid model in more detail. The most damage can be observed in the anterior part of the bone shaft, just proximal of the implant. Approximately the first proximal third of the threads show damage in the medial and lateral bone shaft. The damage of the rigid model is located in a different and much more extensive area.

3.5 Reference Model Osseointegrated - Threaded vs. Unthreaded

In this section the osseointegrated reference model will be compared to the unthreaded osseointegrated model. The differentiation between the models being the implants simplification, one including an axisymmetrical thread, the other does not. Figure 3.31 shows the Load-displacement curve.

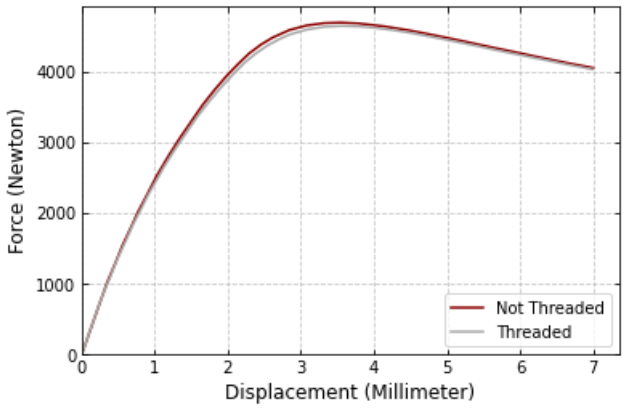

Figure 3.31: Load-displacement curve of the reference osseointegrated model - threaded vs. unthreaded

The simplified implant geometry, shows no notable difference compared to the reference. The ultimate load of the reference model as well as the unthreaded, occurred at a displacement of 3.6mm with a magnitude 4.6kN.

3.5.1 Physiological Load

Figures 3.32 and 3.33 show the deformation and von Mises stress at physiological load in anterior and lateral view.

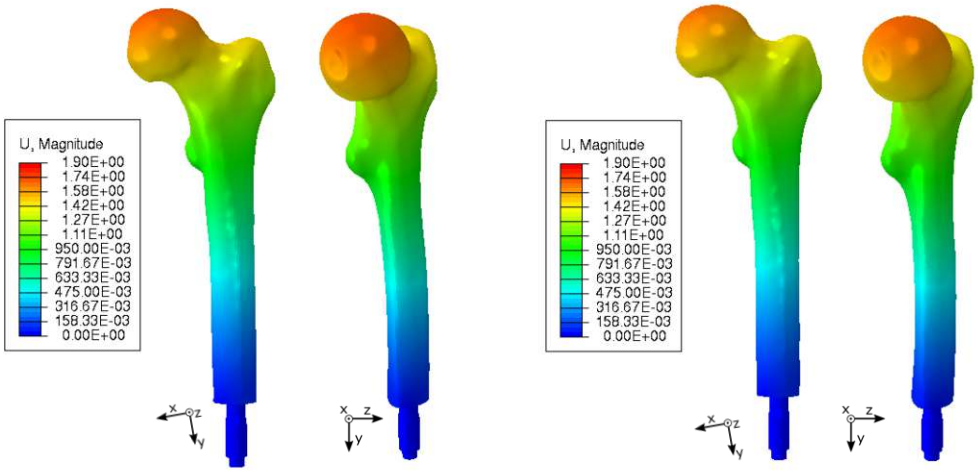

(a) Threaded (c) Unthreaded

Figure 3.32: Deformation at physiological load of the reference osseointegrated model - threaded vs. unthreaded

A slight difference between the threaded and unthreaded model can be seen. The reference model shows a deformation of approximately 1.8 mm in the femur head, whereas the unthreaded model shows a deformation of 1.7 mm. Only the femur head shows a difference, the rest of the deformation does not vary.

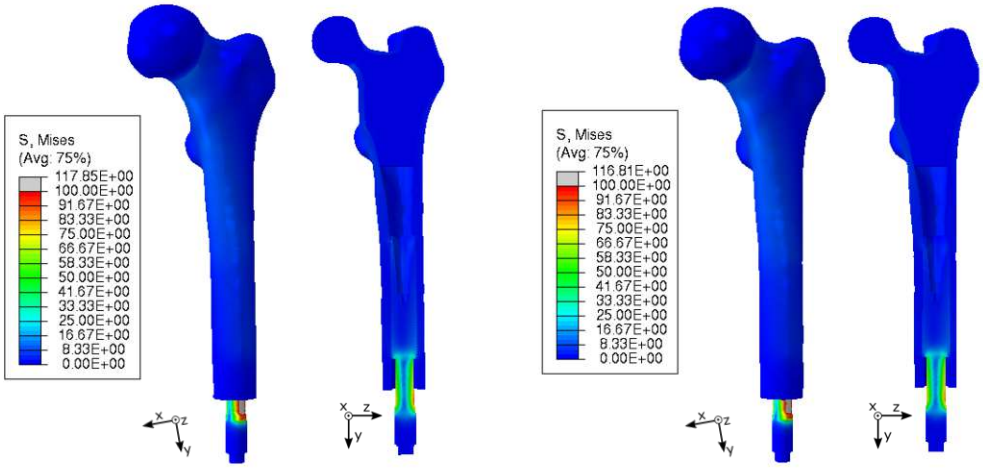

(a) Threaded (c) Unthreaded

Figure 3.33: Stress at physiological load of the reference osseointegrated model - threaded vs. unthreaded

In both models, the highest von Mises stress of both the refrence and unthreaded model, is located at the stem of the implant. There is hardly any difference between the models,

the location as well as the stress magnitude and distribution is very similar.

Figure 3.34 shows the stress in the bone by reducing the colour map by 90%.

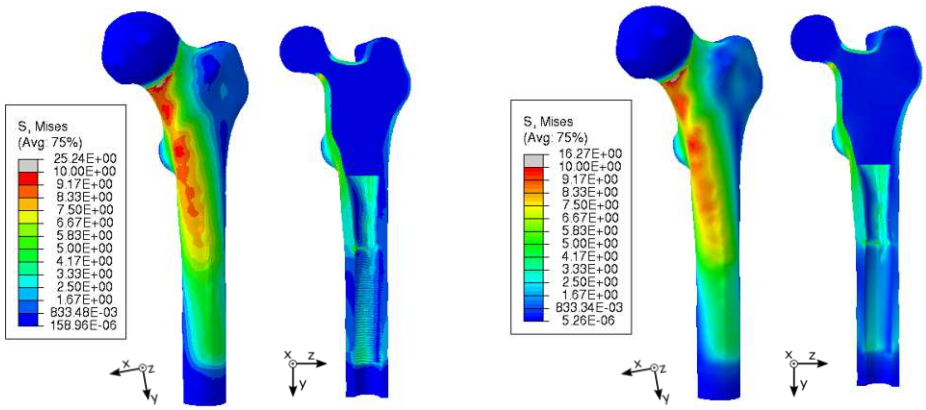

(a) Threaded (c) Unthreaded

Figure 3.34: Stress at physiological load of the reference osseointegrated model - threaded vs. unthreaded

A similar stress distribution can be seen, as the number of elements located at the bone - implant interface region is higher in the reference model, with threads, the von Mises stress distribution in the model without threads appears continuous. The maximum stress value of the unthreaded model is 84% lower.

3.5.2 Ultimate Load

Figures 3.35 and 3.36 show the deformation and von Mises stress at ultimate load in anterior and lateral view.

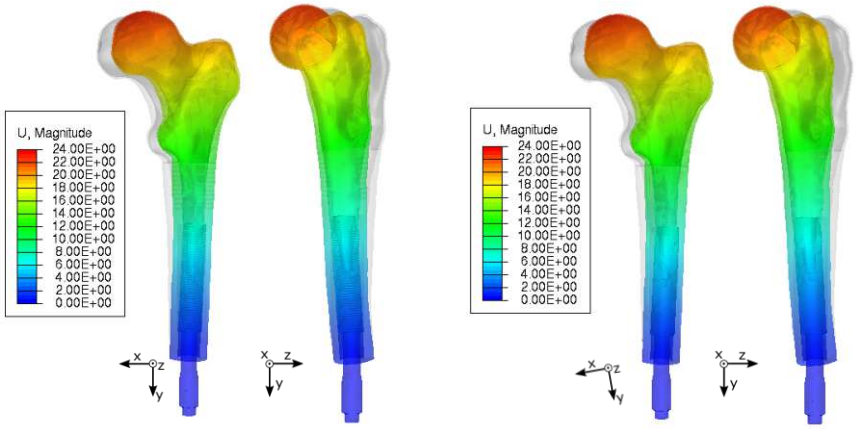

(a) Threaded (c) Unthreaded

Figure 3.35: Deformation at ultimate load of the reference osseointegrated model - threaded vs. unthreaded

The post-implantation and osseointegrated bone/implant, both deformed in lateral, posterior and proximal direction. No difference between the models is visible.

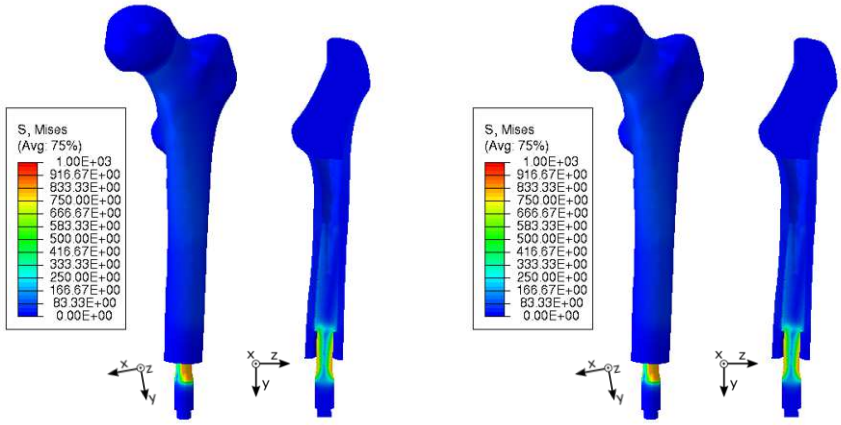

(a) Threaded (c) Unthreaded

Figure 3.36: Stress at ultimate load of the reference osseointegrated model - threaded vs. unthreaded

The highest von Mises stresses of both the reference and unthreaded models, is located at the stem of the implant. No difference between the models is visible.

Figure 3.37 shows the stress within the bone, by scaling the limits of the colour map. The maximum value displayed is 90 MPa, compared the 1000 MPa in Figure 3.37(c).

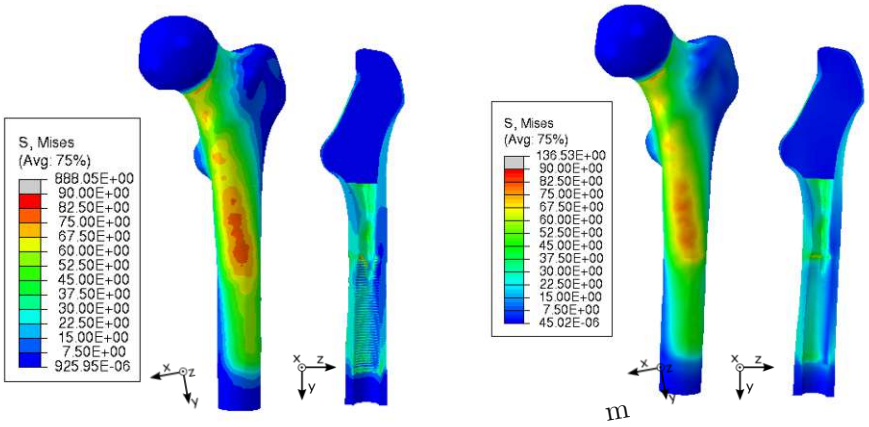

(a) Threaded (c) Unthreaded

Figure 3.37: Stress at ultimate load of the reference osseointegrated model - threaded vs. unthreaded

A similar stress distribution can be seen, even though the maximum value of the unthreaded model is 85% lower.

Figure 3.38 shows the damage plot in posterior view with a coronal cut.

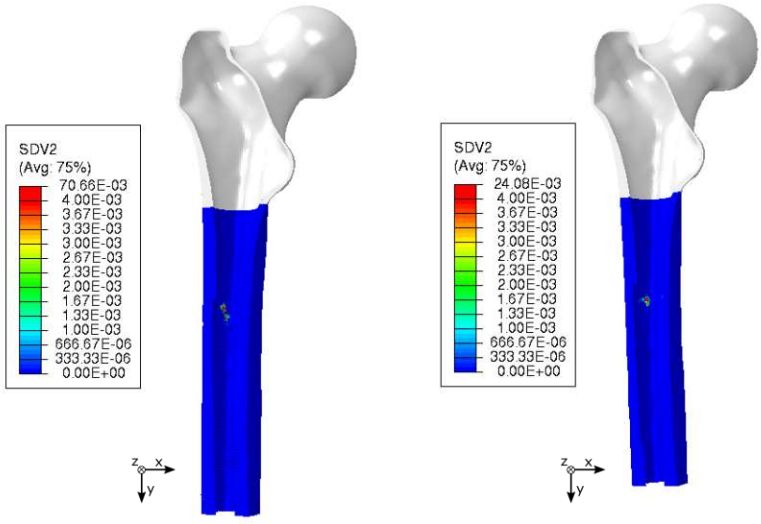

(a) Threaded (b) Unthreaded

Figure 3.38: Bone damage at ultimate load of the reference osseointegrated model - threaded vs. unthreaded

Both models show nearly no damage in the bone.

4 Discussion

The following chapter will be structured according to the previously stated objectives:

(i) *Creation of workflow from CT-data to a FE-model:* Enabling patient-specific models, that predict micromotion and bone/implant failure.

(ii) *Comparison of biomechanical behavior after implantation vs. after osseointegration:* The biomechanical behaviour is predicted both at physiological load and failure.

(iii) *Parameter variation:* Test how simple the model can be to capture the reference models biomechanical behaviour at physiological loading and failure

An additional chapter covering the reference model will be added after the workflow (i), to simplify the comparison of biomechanical behaviour and parameter variation.

4.1 Workflow

The workflow generated in this study enables creating a patient-specific finite element model based on a clinical QCT scan, predicting the biomechanical behaviour during physiological and ultimate loading. The post implantation stage as well as a full osseointegration can be modeled, by using a frictional and tied constraint, in the bone-implant interface. An elasto-viscoplastic damageable bone and elasto-plastic implant material was used in the reference model. The workflow also considers the geometrical impact of the preparation procedure in terms of drilling the tunnel and thread-cutting, even though these processes are not physically modelled. The biomechanical behaviour can be evaluated in terms of the deformation, von Mises stress, damage, micromotion and ultimate load.

This model exceeds the capabilities of those previously presented in literature, such as Tomaszewski et al. [62], Prochor et al. [61] and Thesleff et al. [63] who only used linear material properties and even more simplified bone and implant geometries. However, the model workflow presented herein also has several limitations. In the following sections, the studies used for comparison will not be cited, as the author always refers to the three studies mentioned before.

For instance, the geometry of the bone in this study was a subject-specific CT-based geometry, whereas other studies found in literature used idealized geometries. For instance Prochor et al. and Thesleff et al. modeled the bone as a cylinder. The implant used in this study was simplified by changing the helical threads to axisymmetric threads, making the abutment screw cylindrical and removing geometrical details at the proximal end such as the holes. Tomaszewski et al. and Thesleff et al. completely removed the distal end of the abutment screw, with Tomaszewski et al. using an unthreaded implant including the proximal holes and Thesleff et al. using axisymmetric threads and removing the proximal hole.

In this study the elasto-viscoplastic damageable bone material properties were used in the distal bone region as well as elasto-plastic material for the implant. No other study is known to the author that included material nonlinearties in the simulations of transfermoral osseointegrated prostheses. However, the bone material properties in this study were assumed to be homogeneous in the entire distal region, and assumed to be isotropic throughout the whole model. In contrast, Tomaszewski et al. used linear elastic density dependent material, and other studies even included the anisotropic behaviour of bone

material (e.g., transverly isotropic in Thesleff et al.).

In the study conducted by Tomaszewski et al. the bone was fixed in all spatial directions proximally, whereas a load case measured on transfemoral amputees, including loads and moments was applied. This differed from the boundary conditions used in this thesis, as the distal end was fixed and an axial load was applied proximally, with the intention to allow a future experimental validation. Prochor et al. used a cylinder that was axially loaded with a force of 2 and 4 kN, whereas Theslef et al. applied a force of 1 kN combined with a bending moment of 90 Nm and in a second load case 625 N and 37 Nm. Both Tomaszewski et al. and Prochor et al. modeled the post implantation state with a friction coefficient of 0.4 and the osseointegrated state with a tied constraint, the same as this study. Thesleff et al. only modeled the osseointegrated state with a tied constraint.

In terms of output parameters of the FE models, Tomaszewski et al. looked at the von Mises stress as well as the strain energy density as well as the failure risk, Prochor et al. evaluated the von Mises stress and implant displacement, whereas Thesleff et al. presented the von Mises stress and strain. Given the contact interface and non-linear material constitutive models, this study additionally evaluated the damage and micromotion of the bone-implant system. However, several other parameters that are potentially relevant for successful osseointegration are still not included in these models, such as failure due to fatigue and the adaption of bone to the new mechanical environment (e.g., bone (re-)modelling).

4.2 Reference Model

In the subsequent section the finite element analysis results of the reference model will be discussed in detail. The model has an elasto-plastic threaded implant, frictional constraint between bone and implant, representing the post-implantation state (see section 3.1).

The abutment of the system fails before the bone, which is beneficial, as the bone is not severely damaged. The failure location is as expected, as the implants predetermined breaking point is the abutment [81]. At ultimate load, the deformation in lateral direction was substantially higher than at physiological load. The large deformations can be explained by the yield of the implant, which is further increased by the longer lever arm of the applied load, finally resulting in even higher stresses in the abutment. Even at ultimate load no substantial bone damage occurred, only a few threads were damaged.

The micromotion of the reference model was evaluated at physiological load, resulting in a mean value of 1.5 μm. The micromotion value at which the implant fails, typically referred to in literature, is 150 μm[82]. A systematic review of Kohli et al. [82], suggests that the idea of a universal gold standard for the micromotion is not feasible. Different external factors must be considered, osseointegration with values as high as 750 μm and implant failures as low as 30 μm were reported. Even though the micromotion was lower for the osseointegrated samples, a considerable overlap between the osseointegrated and not osseointegrated groups was reported [82]. The average value at which osseointegration occurred was 112 μm [82], suggesting that the micromotion found in this study is far below the average value and osseointegration of the implant is to be expected.
It must be noted, that only an uniaxial load was evaluated and the micromotion with a more complex load case might vary. Additionally the micromotion might be larger in bones with a thinner cortex.

The ultimate load of the reference model occurred at a displacement of 3.7mm with a magnitude of 4.6 kN. Lee et al. [37] equipped nine transfemoral amputees with prosthesis including load transducers, which were performing daily activities such as walking and ascending and descending stairs. The load and moment patterns along each gait cycle were analysed. No significant load increase when comparing a straight line level gait to climbing stairs could be detected. During a level gait the mean axial force of the patients shows the highest magnitude, approximately 800N. This is far below the herein predicted ultimate load of 4.6 kN. Although no experimental failure loads of the OPRA implant system in human bone were found in literature, there is a study by Barnes et al. [83] who assessed failure loads and micro motion in custom transfemoral implants for osseointegration. They performed a push out test on nine cadaveric human femora, evaluating the micromotion, followed by an axial push out to measure the maximum force. The implants were designed for the study and in the proximal bone interface section was comprised of a lattice structure and solid in the distal end. The mean micromotion and push out force were 3.02 μm and 2099 $\pm$ 499 N.

Based on the model presented in this study a patient-specific ultimate load could be predicted. With the specimen used in the study, the failure load is reasonably high compared to the load applied during gait. As there is a reasonable safety margin to activities common in daily life, it may be suggested that the amputee could start walking without a mechanical failure directly after implantation, therefore reducing the rehabilitation time significantly. This is supported by Tomaszewski et al. [62], who similarly concluded, that loading the implant directly post implantation does not increase the bone failure risk considerably.
In addition, the patient-specific micromotion was predicted by the model presented in this study, and was well below the values reported for implant failure in the literature [82]. A good osseointegration is therefore arguable, keeping in mind the limitation that only one load case, was evaluated.

4.3 Post-Implantation vs. Osseointegration

The subsequent section compares the fully osseointegrated model to the post-implantation, the differentiation being the bone implant interface constraint. A friction constraint was chosen for the post-implantation model, compared to a tied constraint in the osseointegrated representation. Displacement and von Mises stress was evaluated at physiological load, further the bone damage was added at ultimate load.

Hardly any difference between the models can be seen at the structural level. Compared to the osseointegrated model, the post implantation model shows six percent more maximum deformation and two percent more maximum von Mises stress at physiological load. The difference in maximum deformation decreased to one percent, whereas the maximum von Mises stress increased to 6.5% at ultimate load. This is also represented by the Load-displacement curve, where the failure load of both models is 4.6 kN occurring at a displacement of 3.7 mm for the reference model and 3.6 mm for the osseointegrated model.
Therefore when looking at the difference on a structural level, the differences are negligible as the abutment fails first, therefore the screw-bone interface plays a minor role. In the treads on the other a hand, a difference is noticeable due to the different contact constraints. Hence when a detailed analysis of the threads is of interest, for example for

designing an implant to reducing stress on the threads, allowing for optimal osseointegration, the reference model should be used.

The previously mentioned statement that amputees may apply more load onto the implant system earlier during rehabilitation is supported by the fact, that on a structural level the model showed nearly no difference in terms of failure for this particular loading scenario.
In terms of computational modelling, the osseointegrated model offers a good approximation of the reference model for this specific bone - implant system. This suggests that a tied constraint is a viable option for the finite element modeling if thread details are not of interest. Predicting post implantation stability with the osseointegrated model, reduces the modelling effort and also saves computational time.

4.4 Parameter Study: Reference vs. Rigid

The subsequent section compares the reference to the rigid model, the differentiation being the implant material. An elasto-plastic material was chosen for the reference model, whereas the implant was modeled as rigid in the rigid representation. Displacement and von Mises stress was evaluated at physiological load, additionally the bone damage was evaluated at ultimate load.

The failure load difference between the models is significant, this can be seen in the load-displacement curve. The failure load increased by 259%, obviously, the explanation being, that the implant is modeled as rigid hence does not yield.

Similarly a significant difference in deformation and bone damage can be seen, the reason being that the implant can not deform or not yield. The failure is dominated by high stresses in the proximal end of the bone, also being the reason for the high damage in this bone region. In addition geometric effects may play a role, as the force lever in the rigid model is not as high due to the implant not yielding, therefore the bending moment on the abutment is less.

The rigid and reference models, show a significant difference for both the osseointegrated and post-implantation case. Therefore, the simplification of modeling the implant as rigid does not offer a good approximation of the reference model. Note that some studies [84, 85], where micro FE simulations of screw-bone interfaces are modeled, use rigid screws to reduce computational time and found good agreement of their predictions with experimental results. However, this is evidently highly specific on the investigated load case and type of orthopaedic implant. For transfemoral osseointegrated prosthesis, modelling the implant as rigid body cannot be recommended.

4.5 Parameter Study: Threaded vs Unthreaded

The subsequent section compares the reference to the unthreaded model, the differentiation being the implant geometry. An axisymmetric thread was chosen for the reference model, where as the thread was removed in the unthreaded representation. Displacement and von Mises Stress was evaluated at physiological load, further the bone damage was added at ultimate load.

The difference between the models is not significant on a structural level which further confirms the low influence of the screw-bone interface for the mechanical behaviour at the structural level. However, when omitting the threads the detailed information on the stress within the bone - implant interface is lost. Additionally the unthreaded model can only be modeled with a tied constraint at the bone-implant interface, therefore micromotion can not be evaluated.

The results of this study were supported by literature such as Prochor et al. [61], who compared a threaded and an unthreaded, press fitted implant in their finite element study, while applying axial load. After osseointegration, the stress patterns in the bone, as well as the implant axial displacement were similar in the threaded and press fitted case [61]. In the studies of Tomaszewski et al. [59, 62] the implant was also modeled without threads, as the author states the negligible effect of the thread geometry, on the overall bone response to the implant . Thesleff et al. [63] observed that the cortical thickness has a bigger effect on the maximum stress than the thread depth and geometry.

The benefits of on unthreaded model are as mentioned previously, the reduction of elements and therefore computational time. The unthreaded model should be considered, if thread details and micromotion are not of interest in the specific application.

4.6 Limitations

Several limitations of this finite element study must be discussed. Firstly, of all the model is not validated, therefore the clinical relevance is impaired. Secondly, only one specimen was used for the evaluation, therefore results are specimen specific and can not be generalised. Thirdly, the model is limited to isolated bone, as no soft tissue, muscle forces and joints are included, which may have an effect on the stress fields. Also the full complexity of bone tissue is not modeled, as the bone is a living anisotropic and viscoelastic tissue which remodels. Fourthly, the boundary conditions are limited to a uniaxial loading, compared to a complex loading scenario including shear forces and torsion. The uniaxial loading was chosen to facilitate future experimental validation, making it easier to determine failure loads. Fifthly, the geometry was simplified and the preparation procedure (drilling and thread tapping) were only considered geometrically but not in the physical simulation. Finally, the patients typically considered for an OPRA implant are not represented by the specimen used in this study. The age is lower and therefore a higher bone mineral density can be expected, consequently the bone is stronger and less likely to break. This may impact the finite element analysis results, by increasing the failure load.

4.7 Conclusion

This work presented a workflow to create specimen specific FE-models from CT-scans with virtually implanted OPRA system to investigate the mechanical behavior for physiological loads but also until failure. Based on one exemplary bone, it was shown that failure of the bone-implant system was dictated by yield of the abutment rather than failure of the bone or bone-implant interface. The micromotion values at physiological load levels were well below limits reported in literature [82], which should ensure good osseointegration. Ultimate load after osseointegration was similar to the ultimate load directly after implantation, which argues for the possibility of early weight bearing.

The study also compared different FE model simplifications and allows to give modelling

guidelines that may save computational effort depending on the use case. If only deformation and failure load are of interest, even an unthreaded implant geometry and fully tied bone-implant interface can be used. If micromotion and stresses in close proximity to the implant are of interest, the threaded post-implantation reference model with a frictional bone-implant interface must be used. Models with a rigid rather than elasto(-plastic) implant material demonstrate a significantly different biomechanical behavior and therefore, are not considered as a viable modeling option.

In the future, the FE models need to be validated experimentally. If this validation is successful, the models could help to judge the eligibility of patients for bone-anchored transfemoral prostheses and to potentially provide shorter, patient-specific rehabilitation protocol to further improve the quality of life for amputees.

References

[1] E. N. Marieb and K. Hoehn, *Human anatomy & physiology*. Pearson education, 2007.

[2] A. Thesleff, M. Ortiz-Catalan, and R. Brånemark, "Low plasticity burnishing improves fretting fatigue resistance in bone-anchored implants for amputation prostheses," *Medical Engineering & Physics*, vol. 100, p. 103755, 2022.

[3] "Opra fixture biohelix." `https://product.statnano.com/product/10664/opra-fixture-biohelix`. Accessed: 2023-09-02.

[4] Integrum AB, "Opra femur instructions for use. implant system for direct skeletal anchorage of amputation prostheses," Unpublished document provided by the manufacturer.

[5] K. Ziegler-Graham, E. J. MacKenzie, P. L. Ephraim, T. G. Travison, and R. Brookmeyer, "Estimating the prevalence of limb loss in the united states: 2005 to 2050," *Archives of physical medicine and rehabilitation*, vol. 89, no. 3, pp. 422–429, 2008.

[6] R. Sinha and W. J. Van Den Heuvel, "A systematic literature review of quality of life in lower limb amputees," *Disability and rehabilitation*, vol. 33, no. 11, pp. 883–899, 2011.

[7] E. Schaffalitzky, P. Gallagher, M. Maclachlan, and N. Ryall, "Understanding the benefits of prosthetic prescription: exploring the experiences of practitioners and lower limb prosthetic users," *Disability and Rehabilitation*, vol. 33, no. 15-16, pp. 1314–1323, 2011.

[8] C. D. Murray, "Being like everybody else: the personal meanings of being a prosthesis user," *Disability and Rehabilitation*, vol. 31, no. 7, pp. 573–581, 2009.

[9] K. Hagberg, E. Hansson, and R. Brånemark, "Outcome of percutaneous osseointegrated prostheses for patients with unilateral transfemoral amputation at two-year follow-up," *Archives of physical medicine and rehabilitation*, vol. 95, no. 11, pp. 2120–2127, 2014.

[10] C. H. Hansen, R. L. Hansen, P. H. Jørgensen, K. K. Petersen, and A. Norlyk, "The process of becoming a user of an osseointegrated prosthesis following transfemoral amputation: a qualitative study," *Disability and Rehabilitation*, vol. 41, no. 3, pp. 276–283, 2019.

[11] P. Augat, M. W. Hast, G. Schemitsch, M. Heyland, A. Trepczynski, E. Borgiani, G. Russow, S. Märdian, G. N. Duda, M. Hollensteiner, *et al.*, "Biomechanical models: Key considerations in study design," *OTA International*, vol. 4, no. 2S, p. e099, 2021.

[12] C.-L. Tseng, D. Helmer, M. Rajan, A. Tiwari, D. Miller, S. Crystal, M. Safford, J. Greenberg, and L. Pogach, "Evaluation of regional variation in total, major, and minor amputation rates in a national health-care system," *International Journal for Quality in Health Care*, vol. 19, no. 6, pp. 368–376, 2007.

[13] T. R. Dillingham, L. E. Pezzin, and E. J. MacKenzie, "Limb amputation and limb deficiency: epidemiology and recent trends in the united states," *Southern medical journal*, vol. 95, no. 8, pp. 875–884, 2002.

[14] R. H. Meier and D. Melton, "Ideal functional outcomes for amputation levels," *Physical Medicine and Rehabilitation Clinics*, vol. 25, no. 1, pp. 199–212, 2014.

[15] X. Wang, J. Nyman, X. Dong, H. Leng, and M. Reyes, "Fundamental biomechanics in bone tissue engineering," *Synthesis Lectures on Tissue Engineering*, vol. 2, no. 1, pp. 1–225, 2010.

[16] J. P. Goldblatt and J. C. Richmond, "Anatomy and biomechanics of the knee," *Operative Techniques in Sports Medicine*, vol. 11, no. 3, pp. 172–186, 2003.

[17] D. P. Byrne, K. J. Mulhall, and J. F. Baker, "Anatomy & biomechanics of the hip," *The open sports medicine Journal*, vol. 4, no. 1, 2010.

[18] "Anatomy, bony pelvis and lower limb: Femoral muscles." `https://www.ncbi.nlm.nih.gov/books/NBK500008/`. Accessed: 2023-08-28.

[19] J. G. Penn-Barwell, "Outcomes in lower limb amputation following trauma: a systematic review and meta-analysis," *Injury*, vol. 42, no. 12, pp. 1474–1479, 2011.

[20] J. M. P. de Godoy, D. Braile, S. Buzatto, O. Longo, and O. Fontes, "Quality of life after amputation," *Psychology, health & medicine*, vol. 7, no. 4, pp. 397–400, 2002.

[21] H. Senra, R. A. Oliveira, I. Leal, and C. Vieira, "Beyond the body image: a qualitative study on how adults experience lower limb amputation," *Clinical rehabilitation*, vol. 26, no. 2, pp. 180–191, 2012.

[22] M. Hopkins, L. McMenemy, S. Turner, and A. H. McGregor, "Sockets and residuum health," in *Blast Injury Science and Engineering: A Guide for Clinicians and Researchers*, pp. 447–478, Springer, 2023.

[23] B. Welke, C. Hurschler, M. Schwarze, E. Jakubowitz, H.-H. Aschoff, and M. Örgel, "Comparison of conventional socket attachment and bone-anchored prosthesis for persons living with transfemoral amputation-mobility and quality of life," *Clinical Biomechanics*, vol. 105, p. 105954, 2023.

[24] S. L. Kapp, "Transfemoral socket design and suspension options," *Physical Medicine and Rehabilitation Clinics*, vol. 11, no. 3, pp. 569–584, 2000.

[25] I. Long, "Allowing normal adduction of femur in the above-knee amputations," *Orthotics and Prosthetics*, vol. 29, pp. 53–58, 1975.

[26] K. Hagberg and R. Brånemark, "Consequences of non-vascular trans-femoral amputation: A survey of quality of life, prosthetic use and problems," *Prosthetics and orthotics international*, vol. 25, no. 3, pp. 186–194, 2001.

[27] T. Albrektsson, P.-I. Brånemark, H.-A. Hansson, and J. Lindström, "Osseointegrated titanium implants: requirements for ensuring a long-lasting, direct bone-to-implant anchorage in man," *Acta Orthopaedica Scandinavica*, vol. 52, no. 2, pp. 155–170, 1981.

[28] M. B. Zaid, R. J. O'Donnell, B. K. Potter, and J. A. Forsberg, "Orthopaedic osseointegration: state of the art," *JAAOS-Journal of the American Academy of Orthopaedic Surgeons*, vol. 27, no. 22, pp. e977–e985, 2019.

[29] E. Hägström, K. Hagberg, B. Rydevik, and R. Brånemark, "Vibrotactile evaluation: osseointegrated versus socket-suspended transfemoral prostheses.," *Journal of Rehabilitation Research & Development*, vol. 50, no. 10, 2013.

[30] K. Hagberg, R. Brånemark, B. Gunterberg, and B. Rydevik, "Osseointegrated transfemoral amputation prostheses: prospective results of general and condition-specific quality of life in 18 patients at 2-year follow-up," *Prosthetics and orthotics international*, vol. 32, no. 1, pp. 29–41, 2008.

[31] J. G. Tropf and B. K. Potter, "Osseointegration for amputees: Current state of direct skeletal attachment of prostheses," *Orthoplastic Surgery*, 2023.

[32] A. Thesleff, R. Brånemark, B. Håkansson, and M. Ortiz-Catalan, "Biomechanical characterisation of bone-anchored implant systems for amputation limb prostheses: a systematic review," *Annals of biomedical engineering*, vol. 46, no. 3, pp. 377–391, 2018.

[33] Y. Li and R. Brånemark, "Osseointegrated prostheses for rehabilitation following amputation," *Der Unfallchirurg*, vol. 120, no. 4, pp. 285–292, 2017.

[34] R. Brånemark, L. Emanuelsson, A. Palmquist, and P. Thomsen, "Bone response to laser-induced micro-and nano-size titanium surface features," *Nanomedicine: Nanotechnology, Biology and Medicine*, vol. 7, no. 2, pp. 220–227, 2011.

[35] M. Dillon, "Lee, winson and frossard, laurent and brånemark, rickard (2006) loading applied on trans-femoral osseointegrated prostheses. in," 2006.

[36] L. Frossard, N. Stevenson, J. Smeathers, E. Häggström, K. Hagberg, J. Sullivan, D. Ewins, D. L. Gow, S. Gray, and R. Brånemark, "Monitoring of the load regime applied on the osseointegrated fixation of a trans-femoral amputee: a tool for evidence-based practice," *Prosthetics and orthotics international*, vol. 32, no. 1, pp. 68–78, 2008.

[37] W. C. Lee, L. A. Frossard, K. Hagberg, E. Haggstrom, R. Brånemark, J. H. Evans, and M. J. Pearcy, "Kinetics of transfemoral amputees with osseointegrated fixation performing common activities of daily living," *Clinical biomechanics*, vol. 22, no. 6, pp. 665–673, 2007.

[38] L. A. Frossard, R. Tranberg, E. Haggstrom, M. Pearcy, and R. Brånemark, "Load on osseointegrated fixation of a transfemoral amputee during a fall: loading, descent, impact and recovery analysis," *Prosthetics and orthotics international*, vol. 34, no. 1, pp. 85–97, 2010.

[39] L. Frossard, D. L. Gow, K. Hagberg, N. Cairns, B. Contoyannis, S. Gray, R. Brånemark, and M. Pearcy, "Apparatus for monitoring load bearing rehabilitation exercises of a transfemoral amputee fitted with an osseointegrated fixation: a proof-of-concept study," *Gait & posture*, vol. 31, no. 2, pp. 223–228, 2010.

[40] K. Hagberg, R. Brånemark, and O. Hägg, "Questionnaire for persons with a transfemoral amputation (q-tfa): initial validity and reliability of a new outcome measure.," *Journal of Rehabilitation Research & Development*, vol. 41, no. 5, 2004.

[41] R. Branemark, O. Berlin, K. Hagberg, P. Bergh, B. Gunterberg, and B. Rydevik, "A novel osseointegrated percutaneous prosthetic system for the treatment of patients with transfemoral amputation a prospective study of 51 patients," *Bone & Joint Journal*, vol. 96, no. 1, pp. 106–113, 2014.

[42] R. P. Brånemark, K. Hagberg, K. Kulbacka-Ortiz, Ö. Berlin, and B. Rydevik, "Osseointegrated percutaneous prosthetic system for the treatment of patients with transfemoral amputation: a prospective five-year follow-up of patient-reported outcomes and complications," *The Journal of the American Academy of Orthopaedic Surgeons*, vol. 27, no. 16, p. e743, 2019.

[43] H. Van de Meent, M. T. Hopman, and J. P. Frölke, "Walking ability and quality of life in subjects with transfemoral amputation: a comparison of osseointegration with socket prostheses," *Archives of physical medicine and rehabilitation*, vol. 94, no. 11, pp. 2174–2178, 2013.

[44] M. Sielewicz, J. Scholz, and L. Hanslik, "A five year follow-up of 605 cases of the mccl (metal-cancellous cementless lübeck) total hip prosthesis.," *Italian journal of orthopaedics and traumatology*, vol. 15, no. 4, pp. 433–443, 1989.

[45] K. Hagberg, S.-A. G. Jahani, K. Kulbacka-Ortiz, P. Thomsen, H. Malchau, and C. Reinholdt, "A 15-year follow-up of transfemoral amputees with bone-anchored transcutaneous prostheses: mechanical complications and patient-reported outcomes," *The bone & joint journal*, vol. 102, no. 1, pp. 55–63, 2020.

[46] P. T. Pospiech, R. Wendlandt, H.-H. Aschoff, S. Ziegert, and A. P. Schulz, "Quality of life of persons with transfemoral amputation: Comparison of socket prostheses and osseointegrated prostheses," *Prosthetics and orthotics international*, p. 0309364620948649, 2020.

[47] M. Al Muderis, K. Tetsworth, A. Khemka, S. Wilmot, B. Bosley, S. Lord, and V. Glatt, "The osseointegration group of australia accelerated protocol (ogaap-1) for two-stage osseointegrated reconstruction of amputated limbs," *The bone & joint journal*, vol. 98, no. 7, pp. 952–960, 2016.

[48] M. Al Muderis, A. Khemka, S. J. Lord, H. Van de Meent, and J. P. M. Frölke, "Safety of osseointegrated implants for transfemoral amputees: a two-center prospective cohort study," *JBJS*, vol. 98, no. 11, pp. 900–909, 2016.

[49] D. Reetz, R. Atallah, J. Mohamed, H. van de Meent, J. Frölke, and R. Leijendekkers, "Safety and performance of bone-anchored prostheses in persons with a transfemoral amputation: a 5-year follow-up study," *JBJS*, vol. 102, no. 15, pp. 1329–1335, 2020.

[50] J. Tillander, K. Hagberg, Ö. Berlin, L. Hagberg, and R. Brånemark, "Osteomyelitis risk in patients with transfemoral amputations treated with osseointegration prostheses," *Clinical Orthopaedics and Related Research®*, vol. 475, pp. 3100–3108, 2017.

[51] P. Tomaszewski, B. Lasnier, G. Hannink, G. J. Verkerke, and N. Verdonschot, "Experimental assessment of a new direct fixation implant for artificial limbs," *Journal of the mechanical behavior of biomedical materials*, vol. 21, pp. 77–85, 2013.

[52] B. Welke, C. Hurschler, M. Föller, M. Schwarze, and T. Calliess, "Stiffness and ultimate load of osseointegrated prosthesis fixations in the upper and lower extremity," *Biomedical engineering online*, vol. 12, no. 1, pp. 1–13, 2013.

[53] K.-J. Bathe, *Finite element procedures*. Klaus-Jurgen Bathe, 2006.

[54] S. A. Maas, B. J. Ellis, G. A. Ateshian, and J. A. Weiss, "Febio: finite elements for biomechanics," *Journal of biomechanical engineering*, vol. 134, no. 1, p. 011005, 2012.

[55] E. F. Morgan and M. L. Bouxsein, "Use of finite element analysis to assess bone strength," *IBMS BoneKEy*, vol. 2, p. 8, 2005.

[56] D. L. Logan, *A first course in the finite element method*. Cengage Learning, 2011.

[57] F. Taddei, E. Schileo, B. Helgason, L. Cristofolini, and M. Viceconti, "The material mapping strategy influences the accuracy of ct-based finite element models of bones: an evaluation against experimental measurements," *Medical engineering & physics*, vol. 29, no. 9, pp. 973–979, 2007.

[58] C. Krestan and M. Gruber, "Quantitative computertomographie (qct)," *Journal für Mineralstoffwechsel & Muskuloskelettale Erkrankungen*, vol. 20, no. 2, pp. 59–65, 2013.

[59] P. Tomaszewski, M. Van Diest, S. Bulstra, N. Verdonschot, and G. J. Verkerke, "Numerical analysis of an osseointegrated prosthesis fixation with reduced bone failure risk and periprosthetic bone loss," *Journal of biomechanics*, vol. 45, no. 11, pp. 1875–1880, 2012.

[60] P. Tomaszewski, N. Verdonschot, S. Bulstra, and G. Verkerke, "New osseointegrated fixation implant for amputation-prosthesis designed to reduce bone failure risk and periprosthetic bone loss-finite element study," in *Orthopaedic Proceedings*, vol. 94, pp. 192–192, The British Editorial Society of Bone & Joint Surgery, 2012.

[61] P. Prochor, S. Piszczatowski, and E. Sajewicz, "Biomechanical evaluation of a novel limb prosthesis osseointegrated fixation system designed to combine the advantages of interference-fit and threaded solutions," *Acta of Bioengineering and Biomechanics*, vol. 18, no. 4, pp. 21–31, 2016.

[62] P. Tomaszewski, N. Verdonschot, S. Bulstra, and G. Verkerke, "A comparative finite-element analysis of bone failure and load transfer of osseointegrated prostheses fixations," *Annals of biomedical engineering*, vol. 38, pp. 2418–2427, 2010.

[63] A. Thesleff, M. Ortiz-Catalán, and R. Brånemark, "The effect of cortical thickness and thread profile dimensions on stress and strain in bone-anchored implants for amputation prostheses," 2021.

[64] T. D. DenOtter and J. Schubert, "Hounsfield unit," 2019.

[65] D. H. Pahr and P. K. Zysset, "From high-resolution ct data to finite element models: development of an integrated modular framework," *Computer methods in biomechanics and biomedical engineering*, vol. 12, no. 1, pp. 45–57, 2009.

[66] J. J. Schwiedrzik and P. Zysset, "An anisotropic elastic-viscoplastic damage model for bone tissue," *Biomechanics and modeling in mechanobiology*, vol. 12, no. 2, pp. 201–213, 2013.

[67] A. Synek, Y. Chevalier, S. Baumbach, and D. Pahr, "The influence of bone density and anisotropy in finite element models of distal radius fracture osteosynthesis: evaluations and comparison to experiments," *Journal of biomechanics*, vol. 48, no. 15, pp. 4116–4123, 2015.

[68] A. International, *ASM Handbook: Volume 2 - Properties and Selection: Nonferrous Alloys and Special-Purpose Materials*. CITY: ASM International, YEAR.

[69] X. Gao, M. Fraulob, and G. Haïat, "Biomechanical behaviours of the bone–implant interface: a review," *Journal of The Royal Society Interface*, vol. 16, no. 156, p. 20190259, 2019.

[70] M. Ovesy, B. Voumard, and P. Zysset, "A nonlinear homogenized finite element analysis of the primary stability of the bone–implant interface," *Biomechanics and modeling in mechanobiology*, vol. 17, pp. 1471–1480, 2018.

[71] "Orthoload - loading of orthopedic implants." `https://orthoload.com/`. Accessed: 2023-10-30.

[72] G. Bergmann, A. Bender, F. Graichen, J. Dymke, A. Rohlmann, A. Trepczynski, M. O. Heller, and I. Kutzner, "Standardized loads acting in knee implants," *PloS one*, vol. 9, no. 1, p. e86035, 2014.

[73] M. R. Abdul-Kadir, U. Hansen, R. Klabunde, D. Lucas, and A. Amis, "Finite element modelling of primary hip stem stability: the effect of interference fit," *Journal of biomechanics*, vol. 41, no. 3, pp. 587–594, 2008.

[74] I. Levadnyi, J. Awrejcewicz, M. F. Goethel, and A. Loskutov, "Influence of the fixation region of a press–fit hip endoprosthesis on the stress–strain state of the "bone–implant" system," *Computers in Biology and Medicine*, vol. 84, pp. 195–204, 2017.

[75] S. E. Basler, J. Traxler, R. Müller, and G. H. van Lenthe, "Peri-implant bone microstructure determines dynamic implant cut-out," *Medical engineering & physics*, vol. 35, no. 10, pp. 1442–1449, 2013.

[76] N. Lioubavina-Hack, N. P. Lang, and T. Karring, "Significance of primary stability for osseointegration of dental implants," *Clinical oral implants research*, vol. 17, no. 3, pp. 244–250, 2006.

[77] D. Ruffoni, R. Müller, and G. H. van Lenthe, "Mechanisms of reduced implant stability in osteoporotic bone," *Biomechanics and modeling in mechanobiology*, vol. 11, pp. 313–323, 2012.

[78] Q. Zhang, S. Tan, and S. Chou, "Investigation of fixation screw pull-out strength on human spine," *Journal of biomechanics*, vol. 37, no. 4, pp. 479–485, 2004.

[79] V. Chappuis, O. Engel, M. Reyes, K. Shahim, L.-P. Nolte, and D. Buser, "Ridge alterations post-extraction in the esthetic zone: a 3d analysis with cbct," *Journal of dental research*, vol. 92, no. 12_suppl, pp. 195S–201S, 2013.

[80] G. Haiat, H.-L. Wang, and J. Brunski, "Effects of biomechanical properties of the bone–implant interface on dental implant stability: from in silico approaches to the patient's mouth," *Annual Review of Biomedical Engineering*, vol. 16, pp. 187–213, 2014.

[81] H. Grundei, T. Von Stein, D. Schulte-Bockhof, C. Kausch, H. Gollwitzer, and R. Gradinger, "Die endo-exo-femurprothese-update eines versorgungskonzeptes zur rehabilitation von oberschenkelamputierten," *Orthopädie-Technik*, vol. 3, no. 09, pp. 143–149, 2009.

[82] N. Kohli, J. C. Stoddart, and R. J. van Arkel, "The limit of tolerable micromotion for implant osseointegration: a systematic review," *Scientific Reports*, vol. 11, no. 1, pp. 1–11, 2021.

[83] S. C. Barnes, J. C. Clasper, A. M. Bull, and J. R. Jeffers, "Micromotion and push-out evaluation of an additive manufactured implant for above-the-knee amputees," *Journal of Orthopaedic Research®*, vol. 37, no. 10, pp. 2104–2111, 2019.

[84] V. C. Panagiotopoulou, M. Ovesy, B. Gueorguiev, R. G. Richards, P. Zysset, and P. Varga, "Experimental and numerical investigation of secondary screw perforation in the human proximal humerus," *Journal of the mechanical behavior of biomedical materials*, vol. 116, p. 104344, 2021.

[85] M. Ovesy, M. Indermaur, and P. K. Zysset, "Prediction of insertion torque and stiffness of a dental implant in bovine trabecular bone using explicit micro-finite element analysis," *Journal of the mechanical behavior of biomedical materials*, vol. 98, pp. 301–310, 2019.